scientific reports

Check for updates

OPEN

Digital framework for georeferenced multiplatform surveillance of banana wilt using human in the loop AI and YOLO foundation models

Juan Jose Mora[1], Guy Blomme[2], Nancy Safari[3], Sivalingam Elayabalan[4], Ramasamy Selvarajan[5] & Michael Gomez Selvaraj[1]✉

Bananas (*Musa* spp.) are a critical global food crop, providing a primary source of nutrition for millions of people. Traditional methods for disease monitoring and detection are often time-consuming, labor-intensive, and prone to inaccuracies. This study introduces an AI-powered multiplatform georeferenced surveillance system designed to enhance the detection and management of banana wilt diseases. We developed and evaluated several deep learning foundation models, including YOLO-NAS, YOLOv8, YOLOv9, and Faster-RCNN to perform accurate disease detection on both platforms. Our results demonstrate the superior performance of YOLOv9 in detecting healthy, Fusarium Wilt and Xanthomonas Wilt diseased plants in aerial images, achieving high mAP@50, precision and recall metrics ranging from 55 to 86%. In terms of ground level images, we organized the dataset based on disease occurrence in Africa, Latin America, India, Asia and Australia. For this platform, YOLOv8 outperforms the rest and achieves mAP@50, precision and recall between 65 and 99% depending on the plant part and region. Additionally, we incorporated Explainable AI techniques, such as Gradient-weighted Class Activation Mapping, to enhance model transparency and trustworthiness. Human in the Loop Artificial Intelligence was also utilized to enhance the ground level model's predictions.

Bananas (*Musa* spp.) rank as the fourth most important food crop globally, both as a vital food source and significant fruit crop in terms of trade and production volume[1,2] . Their high yields and carbohydrate content make them a crucial daily energy source for people in developing countries, significantly contributing to food security[3,4].

In East Africa, approximately 20 million people, depend on bananas as a dietary staple, while in West and Central Africa, this number rises to around 70 million[5]. The Latin American and Caribbean (LAC) region further illustrates the economic importance of bananas, accounting for about 66% of global exports of Cavendish bananas (*Musa* AAA), with Ecuador as the top exporter. Additionally, the LAC region is a major exporter of plantains, contributing to 72% of the global trade. Despite these high export figures, 62% of banana and plantain production in LAC (20 million tons) is consumed domestically, highlighting their crucial role in regional diets and food security[6]. In other regions such as Australia, bananas are the top-selling supermarket product and the second-largest horticulture industry[7]. The Asia–Pacific region, particularly India, China, and the Philippines, have been major players in banana production for centuries, contributing to over 45% of the world's total production[8,9]. This long-standing cultivation underscores the significant role bananas play in the economies and food security of these countries.

Unfortunately, banana production faces significant challenges from various biotic stresses, including bacterial, viral, and fungal diseases, along with pests. Fungal diseases like black Sigatoka or Black leaf streak *(Mycosphaerella fijiensis*) and Fusarium wilt (*Fusarium oxysporum f. sp. cubense*) are considered the most critical banana diseases worldwide. Additionally, bunchy top disease caused by the banana bunchy top virus (genus

[1]Alliance of Bioversity International and International Center for Tropical Agriculture (CIAT), Km 17 Recta Cali-Palmira, Cali, Colombia. [2]Bioversity International, c/o ILRI, P.O. Box 5689, Addis Ababa, Ethiopia. [3]Bioversity International, Bukavu, South Kivu, Democratic Republic of Congo. [4]Imayam Institute of Agriculture and Technology (IIAT), Affiliated With Tamil Nadu Agricultural University (TNAU), Tiruchirappalli, Tamil Nadu, India. [5]ICAR-National Research Centre for Banana, Tiruchirappalli, Tamil Nadu, India. ✉email: m.selvaraj@cgiar.org

Babuvirus) has emerged as a major constraint on banana production in Asia and Sub-Saharan Africa[10]. The spread of BBTV has been documented in at least six countries in the past ten years, with outbreaks first identified in Benin in 2011 and subsequently in West Africa and East Africa (particularly Uganda and Tanzania)[10,11]. Bacterial diseases like Xanthomonas Wilt (*Xanthomonas vasicola* pv. *musacearum*) in Africa, Banana Blood Disease (*Ralstonia syzygii* subsp. *celebesensis*) in Southeast Asia, and Moko (*Ralstonia solanacearum*) in Latin America further reduce yields and increase crop management expenses. These diseases, pose a serious threat to banana production worldwide.

Monitoring, recording, and mapping the spread of these diseases is essential for enabling targeted interventions and anticipating/mitigating food insecurity risks. However, traditional disease surveillance methods reliant on teams of trained agriculturalists to visit cultivation areas are time-consuming, tedious, expensive, and often inadequate[12]. These methods suffer from a shortage of trained staff, logistical challenges, and the time-consuming process of compiling paper reports. Furthermore, these approaches frequently lead to inaccurate observations due to subjectivity and limitations in data collection[12,13]. Clearly, a more efficient and precise solution is needed to safeguard global banana production and the well-being of banana farmers.

To address these challenges in disease surveillance and improve the monitoring of banana crops, innovative and technology-driven solutions are necessary. The incorporation of cutting-edge methodologies like remote sensing, digital imaging, disease mapping, and data analytics holds significant potential to revolutionize the landscape of disease identification and monitoring in agriculture[14].

Remote sensing tools such as agricultural drones or unmanned aerial vehicles (UAVs) have emerged as ideal technologies for evaluating crop yields, assessing crop health, and conducting economic evaluations[15]. Additionally, artificial intelligence (AI) and deep learning models have revolutionized crop disease classification, achieving remarkable accuracy in image processing and object detection[16]. AI-based deep learning models have transformed plant disease diagnosis, with researchers increasingly using them to identify and categorize diseases in major crops such as rice, wheat, maize, tomato, citrus, and sugarcane[17–28].

In banana, AI has significantly contributed to various aspects, including crop type classification, leaf disease detection and classification, pest incidence prediction, ripeness stage classification, quality grading prediction, and crop yield forecasting. Specifically, for disease detection, several studies have explored the potential of AI. Selvaraj et al.[29] proposed the Tumaini smartphone app, an AI-based system utilizing deep convolutional neural networks (DCNN) and transfer learning to detect diseases and pests in banana crops. Brown et al.[30] focused on classifying banana leaf diseases using a KNN classifier combined with a custom Gabor filter for feature extraction. Chaudhari et al.[31] identified banana plant diseases by extracting color, shape, and texture features from images and employing a Support Vector Machine (SVM) for classification, achieving an average accuracy of 85% in identifying four diseases: black Sigatoka, Cucumber Mosaic Virus, Banana Bacterial wilt, and Fusarium wilt. Genet et al.[32] employed transfer learning for detecting banana plant leaf images, achieving an impressive classification accuracy with the VGG16 model. Sangeetha et al.[33] proposed an improved method for predicting Fusarium wilt disease using an agro deep learning algorithm, outperforming previous methods.

Advancements in object detection have led to two primary architectures: Two-stage models like Faster-RCNN prioritizing accuracy, and one-stage models like YOLOv8, YOLO-NAS, and the newly released YOLOv9 emphasizing speed[36]. All pretrained models have been applied to various agricultural AI projects, including disease and pest detection in crops like rice, roses, sweet peppers, grapes and bananas[31,34,38–42] as well as tomato ripeness classification and counting[35,44].

The combination of UAVs and deep learning models has shown promise in banana disease detection. Calou et al.[36] Selvaraj et al.[14] Brown et al.[37] Neupane et al.[38] Mora et al.[39] Zhang et al.[40] Aliff et al.[41] have utilized diverse approaches, including RetinaNet, Heap Auto Encoders (HAEs), Faster-RCNN, and YOLOv8, along with various image types (RGB, multispectral) to detect diseases such as black Sigatoka, banana bunchy top disease (BBTD), Xanthomonas Wilt (BXW), fusarium wilt, yellow Sigatoka, banana stem weevil, banana aphid, bacterial soft rot, and Panama disease. These studies highlight the potential of UAV-based solutions for accurate and efficient disease monitoring in banana plantations.

Research and commercial approaches for deploying AI-powered disease detection and mapping systems are also progressing. Platforms like Pestdisplace[42], a research-based platform for monitoring pests and diseases occurrence, and Estamos Alerta[43], a UAV-based deep learning platform for monitoring banana disease in Ecuador are examples of emerging solutions. Private companies such as EOS Data Analytics and Plantix offer satellite-based crop classification and monitoring solutions[44], while Plantix and Agri.io provide crop advisory apps with disease detection and treatment recommendations[45,46].

The need for transparent and globally accessible disease surveillance systems is crucial, particularly, for low-income countries. Such systems, powered by data mining, analysis, information sharing, and modeling, can empower National Plant Protection Organizations (NPPO) and producers/farmers to respond quickly to emerging disease threats, stabilizing food supplies[47]. Integrating UAVs with AI smartphone apps, as proposed in previous studies, holds promise for developing advanced early warning systems across banana production landscapes[29,48].

To enhance transparency and trust, Human-in-the-Loop Machine Learning (HILML) or Human-in-the-Loop AI (HILAI) approaches, Explainable AI (XAI), Usable AI, and Useful AI, are essential[49]. HILAI emphasizes the collaboration between humans and computers, while XAI improves model interpretability. Usable and Useful AI focus on user experience and interaction design.

While Human-in-the-Loop (HIL) techniques have been applied in agriculture for tasks like crop disease detection, their integration with UAVs and crop surveillance systems for banana plants remain underexplored. This research addresses this gap by developing a robust and user-friendly AI system for banana disease detection[64–67].

Type	Images collected	Whole annotations		
UAV-RGB	6854	Healthy	Xanthomonas Wilt	Fusarium Wilt
		14,238	4436	4874

Table 1. Description of annotated UAV banana datasets used in this study.

Classes	Images collected							Whole annotations						
Plant Part	Rachis	Cut fruit	Whole plant	Leaf	Bunch	Pseudostem	Corm	Rachis	Cut Fruit	Whole Plant	Leaf	Bunch	Pseudostem	Corm
Healthy	1065	880	1009	915	1154	1061	845	1065	4242	1316	3450	1883	1065	847
Xanthomonas Wilt	–	866	956	898	928	1555	–	–	5577	1053	1174	938	1617	–
Fusarium Wilt	–	–	1350	1498	–	1191	–	–	–	1374	2916	–	1208	–
Bunchy Top Virus	–	–	861	–	–	–	–	–	–	1230	–	–	–	–
Black Sigatoka	–	–		843	–	–	–	–	–		1103	–	–	–
Moko	971	876	1044	1012	954	1626	–	977	5596	1161	1413	964	1695	–
Banana Blood Disease	964	957	–	–	–	–	–	970	6086	–	–	–	–	–
Black Sigatoka + Yellow Sigatoka	–	–	–	1257	–	–	–	–	–	–	1544	–	–	–
Bacterial Wilt	–	1833	1044	1012	954	1626	–	–	11,682	1161	1413	964	1695	–
Corm Weevil	–	–	–	–	–	–	858	–	–	–	–	–	–	884
Total	3000	5412	6264	7435	3990	7059	1703	3012	33,183	7295	13,013	4749	7280	1731

Table 2. Description of annotated ground level banana datasets used in this study.

Therefore, this study aims to recognize the promising potential of Human-in-the-Loop AI (HILAI) techniques within a multisensory AI-powered system for banana disease monitoring. Our research seeks to develop effective and practical solutions for managing diverse banana diseases at field level worldwide. We achieve this by focusing on the following key objectives:

1. To create a rich and extensive dataset encompassing a wide range of common banana diseases using both ground-level and aerial images from banana-producing regions across the globe.
2. To develop customized object detection models based on Faster-RCNN and YOLO-based architectures. These models will be specifically designed to identify banana diseases from images of different plant parts, captured using various platforms (Ground Level & UAV).
3. To determine the most effective framework for high-accuracy disease detection, we rigorously evaluate Faster-RCNN and three YOLO architectures (YOLO-NAS, YOLOv8, and YOLOv9). Robust evaluation metrics will ensure a comprehensive assessment.
4. To enhance the Tumaini smartphone App's user experience and incorporate Human-in-the-Loop AI (HILAI) principles, providing a more transparent and user-friendly experience.
5. To integrate the developed app with an online platform for disease mapping, enabling proactive disease control and management strategies. The Deep Learning pipeline (DLOPs) will undergo real-world field testing to validate its capabilities in practical scenarios.

Materials and methods

Description of deep learning multiplatform system approach

Our Deep Learning (DL) surveillance system comprises an aerial and a ground-level platform, each tailored for distinct phases of plant disease detection and surveillance process.

The aerial platform is leveraged for scanning extensive agricultural areas, providing insights into the field's overall health status as well as identifying symptomatic plants resembling those affected by Fusarium Wilt and Xanthomonas Wilt. It employs an aerial model trained on a dataset of images collected via unmanned aerial vehicles (UAVs), categorized into three distinct classes: Healthy, Fusarium Wilt, and Xanthomonas Wilt (Fig. 5a,b).

Conversely, the ground-level platform is engineered to validate the diagnoses of plants initially scanned by the aerial system. This verification is conducted through a deep learning object detection model, which is integrated within a smartphone application. While the aerial platform excels at scanning large areas, ground-level images offer higher resolution and provide easier access to various parts of the plant, allowing for a more comprehensive confirmation of a wider array of diseases. Unlike the aerial system, which focuses primarily on diseases visible in the plant canopy, the ground-level platform can detect symptoms across multiple plant parts. This platform meticulously categorizes nine prevalent banana diseases, which are distributed across five continents and manifest in seven different parts of the plant, including leaves, pseudostems, bunches, and fruits. Each disease and its healthy counterparts are documented in Tables 1 and 2.

For a comprehensive understanding of our DL system's processing architecture and the operational workflow of both platforms, please refer to Fig. 1. This system is meticulously designed to optimize the processing of large-scale areas, ensuring robust and accurate disease detection and classification through the ground-level platform.

Model architectures

YOLOv8, YOLOv9, YOLO-NAS, represent successive advancements in the YOLO family of real-time object detection models, each introducing significant improvements in structure and performance.

YOLOv8, released by Ultralytics in January 2023, incorporates an anchor-free model and a decoupled head, which independently processes objectness, classification, and regression tasks. Its C2f. module, modified CSPDarknet53 backbone, and spatial pyramid pooling fast (SPPF) layer, and feature extraction[53]. Building on this progress, YOLOv9 leverages the robust codebase of YOLOv5 and marks a significant leap in efficiency and adaptability. Featuring innovations such as Programmable Gradient Information (PGI) and the Generalized Efficient Layer Aggregation Network (GELAN), YOLOv9 enhances the model's capability to process complex visual data more effectively, showcasing improvements in both speed and accuracy[54]. In contrast, YOLO-NAS, utilizing AutoNAC, optimizes architecture for accuracy-latency tradeoffs. Hybrid quantization and attention mechanisms enhance detection capabilities while minimizing information loss and latency[55]. Faster-RCNN distinguishes itself from other object detection models, such as the YOLO series, through its two-stage detection process. Faster-RCNN enables accurate object localization, beneficial for detailed analysis, such as medical imaging and complex scene understanding[56]. While Faster-RCNN often achieves higher accuracy than single-stage detectors like YOLO, it is slower due to its more complex architecture, making it more suitable for scenarios where detection accuracy is prioritized over real-time processing speed[56].

Our study involved training models for both aerial and ground-level imaging platforms. For the aerial platform, we explored four distinct convolutional neural network (CNN) architectures: YOLOv8, YOLOv9, YOLO-NAS, and Faster-RCNN. For the ground-level platform, we initially trained models for the pseudostem and whole plant datasets using YOLOv8, YOLO-NAS, and Faster-RCNN architectures. Later, we evaluated these models to select the most effective architecture. The chosen architecture was subsequently used to train an additional 33 models tailored for ground-level plant parts. These models spanned a comprehensive array of 35 specific datasets including corm, rachis, leaf, cut fruit, whole plant, pseudostem, and bunch across Africa Latin America, India, South East Asia, and Australia..

Dataset collection

Aerial platform

The research targeted landscapes in the northeastern Kabare district, South Kivu province, in the Eastern Democratic Republic of Congo (DR Congo), adversely impacted by Xanthomonas Wilt (BXW) of banana. These areas were specifically selected due to clear disease manifestations, such as leaf yellowing and wilting, premature ripening of fruit, and the secretion of a yellow ooze from cut pseudostems and leaf petioles, as depicted in Fig. 2.

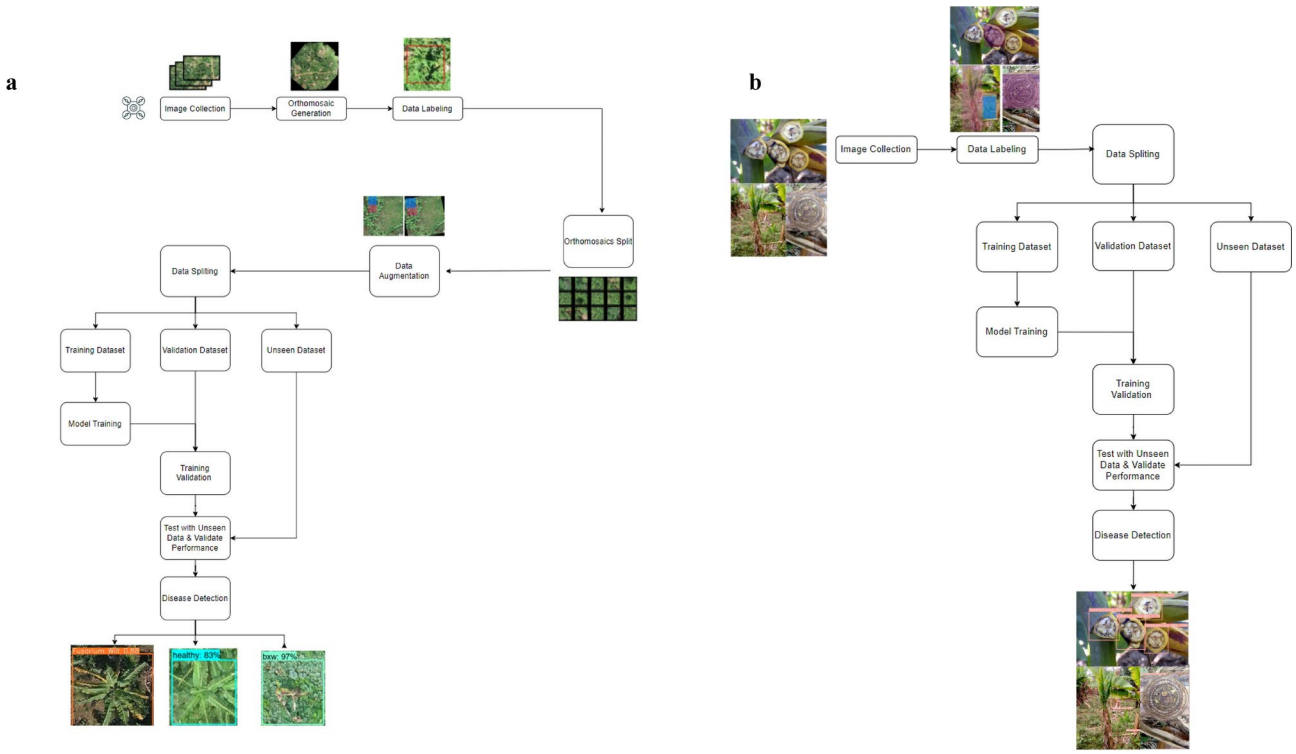

Fig. 1. Overview of DL pipeline for. (**a**) Aerial platform, (**b**) Ground level platform.

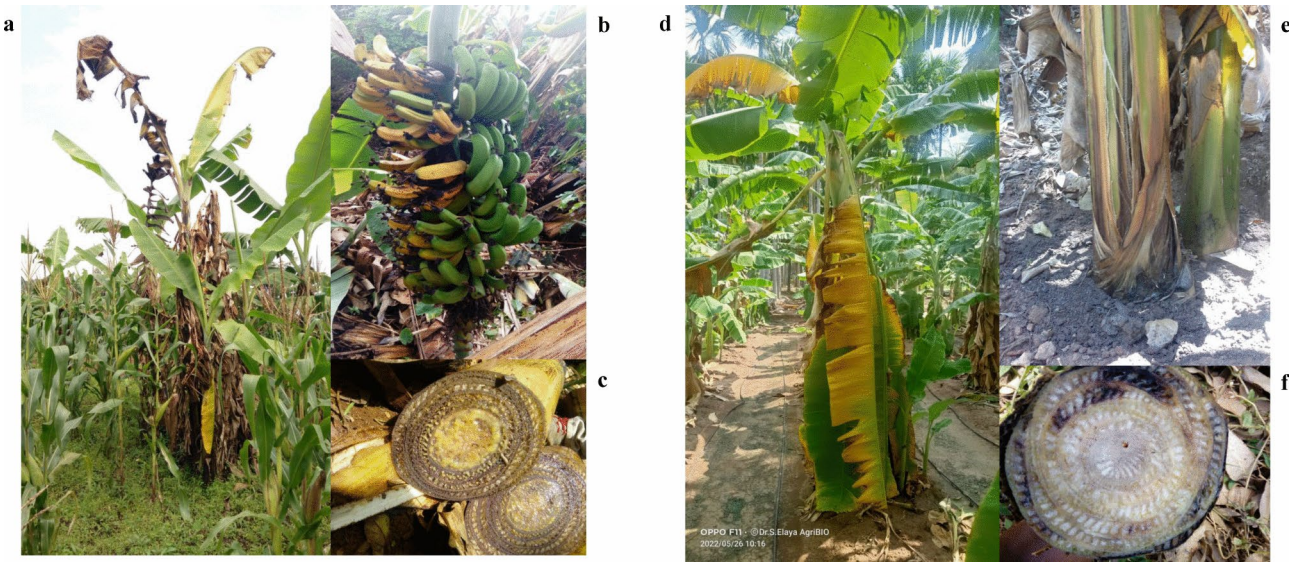

Fig. 2. Real field Images of Xanthomonas (BXW) and Fusarium Wilt (FW). (**a**) BXW Whole Plant, (**b**) BXW premature bunch ripening, (**c**) BXW Oozing Pseudostem, (**d**) FW Whole Plant, (**e**) FW longitudinal splitting of pseudostem, (**f**) FW internal pseudostem.

Camera	Sensor	Radiometric resolution	Spectral resolution—bands	Flight height (m)	Spatial resolution (cm)
DJI-FC6310	RGB—visible	8 bits	3 bands Red (R) Green (G) Blue (B)	60	1.36
20MP Hasselblad L1D-20c camera	RGB—visible	8 bits	3 bands Red (R) Green (G) Blue (B)	60	1.21

Table 3. UAV camera sensors and flight characteristics.

Between 2019 and 2022, field surveys were conducted in 21 banana plantations to collect reliable ground-truth data on BXW's prevalence and characteristics. Experts meticulously examined individual plants at designated sampling sites, classifying them based on observed symptoms into categories of healthy or BXW-infected.

Concurrently, a similar methodology was employed for studying Fusarium wilt in banana plantations near Hanoi, northern Vietnam, with the data collection phase spanning from 2022 to 2023. These surveys focused on plants displaying Fusarium wilt symptoms, including wilting, yellowing of outer/oldest leaves, and pseudostem longitudinal splitting such as the ones seen in Fig. 2.

High-resolution field imagery was captured using a DJI-FC6310 RGB camera mounted on a DJI Phantom 4 Pro (P4P) drone and a DJI Mavic Pro 2 for African and Asian fields, respectively. Flight operations were managed via the Pix4Dcapture app, facilitating automated and efficient flight planning. The drone maintained a steady speed of 2.5 m/s and an altitude of 60 m to adapt to various aerial conditions. Comprehensive details on the camera specifications and drone operational parameters are provided in Table 3.

Ground level platform

Our study utilized a comprehensive dataset from the CGIAR banana image library, which encompasses real field images meticulously collected and curated by banana experts. This extensive collection was sourced from multiple prestigious agricultural research organizations, including Bioversity International (Africa), Tamil Nadu Agricultural University (TNAU) (Southern India), Agrocalidad (Ecuador), Agrosavia (Colombia), and the National Autonomous Institute for Agricultural Investigation (INIAP) (Peru).

The dataset captured a wide array of environmental conditions, reflecting the diverse climates and ecological settings of banana farms in disease and pest hotspots. These locations, depicted in Fig. 3, span Africa (Eastern Democratic Republic of Congo, Central Uganda, Burundi, and Benin); Southern India (Tamil Nadu and Kerala); and provinces in Ecuador (Los Rios, Carchi, El Oro, Manabí, Sucumbíos), Peru (Piura) and Colombia (Magdalena). This geographic and environmental diversity strengthens our model's robustness, allowing for accurate classification and prediction of banana plant health issues under varied global conditions.

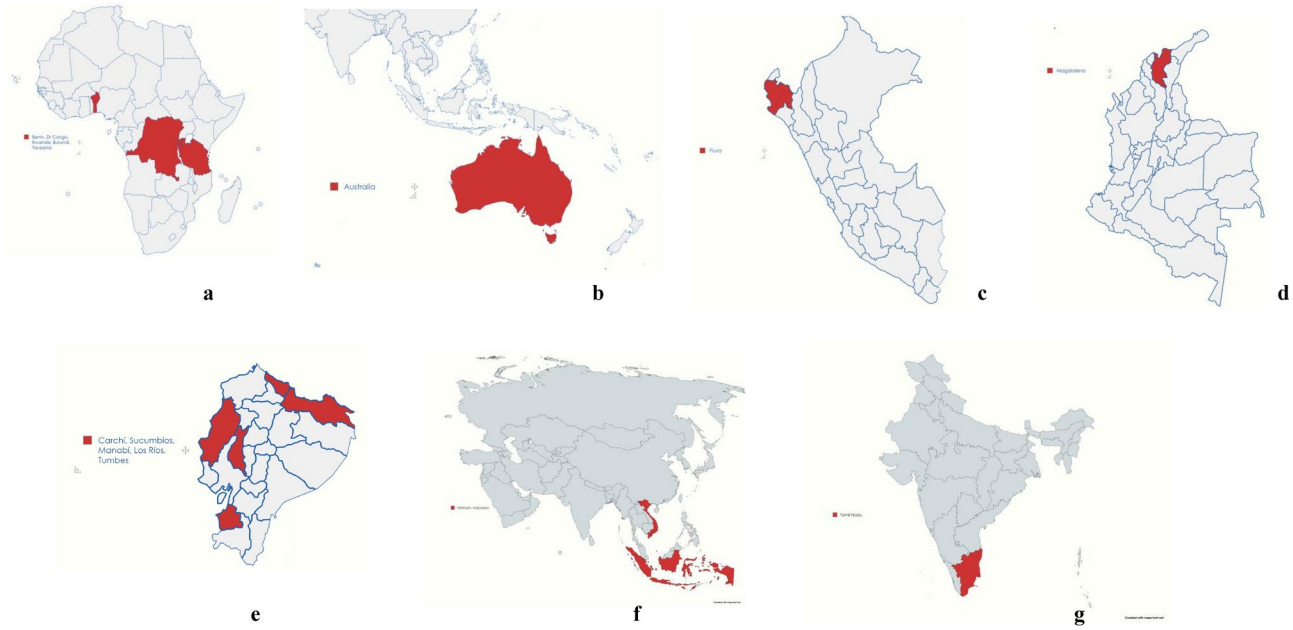

Fig. 3. Geographic Representation of Image Collection. (**a**) Africa, (**b**) Australia, (**c**) Peru, (**d**) Colombia, (**e**) Ecuador, (**f**) South East Asia, (**g**) India

Dataset composition of ground level platform

The dataset incorporates images captured with different devices (cell phones, tablets, standard RGB cameras) under varying lighting conditions and seasons. This rich variety of visual inputs is crucial for training deep learning models. It ensures the models can effectively recognize symptoms across different light settings, seasons, and camera technologies encountered in real-world agricultural settings.

This dataset encompasses images of healthy banana plants alongside those affected by six major diseases—Xanthomonas wilt of banana (BXW), Fusarium wilt of banana (FWB), Black Sigatoka (BS), Banana Bunchy Top Disease (BBTD), Banana Blood Disease (BBD, Moko along with one major pest, the Banana Corm Weevil (BCW). Additionally, it features two combined classes—Black Sigatoka + Yellow Sigatoka (BYS) and Bacterial Wilt (BW)—with the latter consisting of images from the BXW, BBD, and Moko classes, aimed at alerting countries like India or Australia of a potential new bacterial wilt introduction. Moreover, to address the variability in symptom manifestation across different parts of the plant, the dataset includes images from seven distinct plant parts: the leaf, rachis, pseudostem, whole plant, corm, bunch, and transversally cut fruit.

To address the uneven global distribution of banana diseases and their overlapping symptoms, we organized our image library systematically by region, disease/pest, and plant part. Each regional dataset, as illustrated in Fig. 4, is curated to focus on the diseases prevalent in that specific area. Notably, while the datasets are tailored to regional disease profiles, the images themselves are not always sourced directly from those regions. This structured approach enables the development and validation of deep learning models that are finely tuned to the unique agricultural challenges faced by banana growers in different parts of the world. We then evaluate the performance of these region-specific models to ensure their effectiveness in addressing the diseases relevant to each region.

Dataset annotation

Our dataset underwent a manual annotation process using 'LabelImg' software. Banana Experts meticulously drew bounding boxes around symptomatic regions on both aerial and ground-level images, as depicted in Fig. 5. These marked areas corresponded to regions exhibiting signs of disease or pest infestation. Following this process, images were assigned to specific class labels for various diseases or pests present. This rigorous annotation process ensured highly accurate data for training our models and facilitated precise symptom localization, which is critical for effective disease and pest detection. The annotated data for each image was then saved in XML format. This format preserved detailed information such as bounding box coordinates and class labels.

To accommodate the input requirements of our deep learning models, particularly those using the You Only Look Once (YOLO) architectures for object detection, the XML files were converted into YOLO format. This conversion streamlined the annotation data into a text format that delineated the bounding boxes and class labels, specifically designed for the YOLO system. The collected dataset provides a valuable resource for developing and training machine learning models for banana disease detection. For the aerial images, unlike other studies, our approach ensured that each plant in the dataset was fully annotated to avoid the negative impact on model performance metrics that can result from using partially annotated images[39]. This thorough annotation process enhances the accuracy of disease identification and characterization within the aerial imagery.

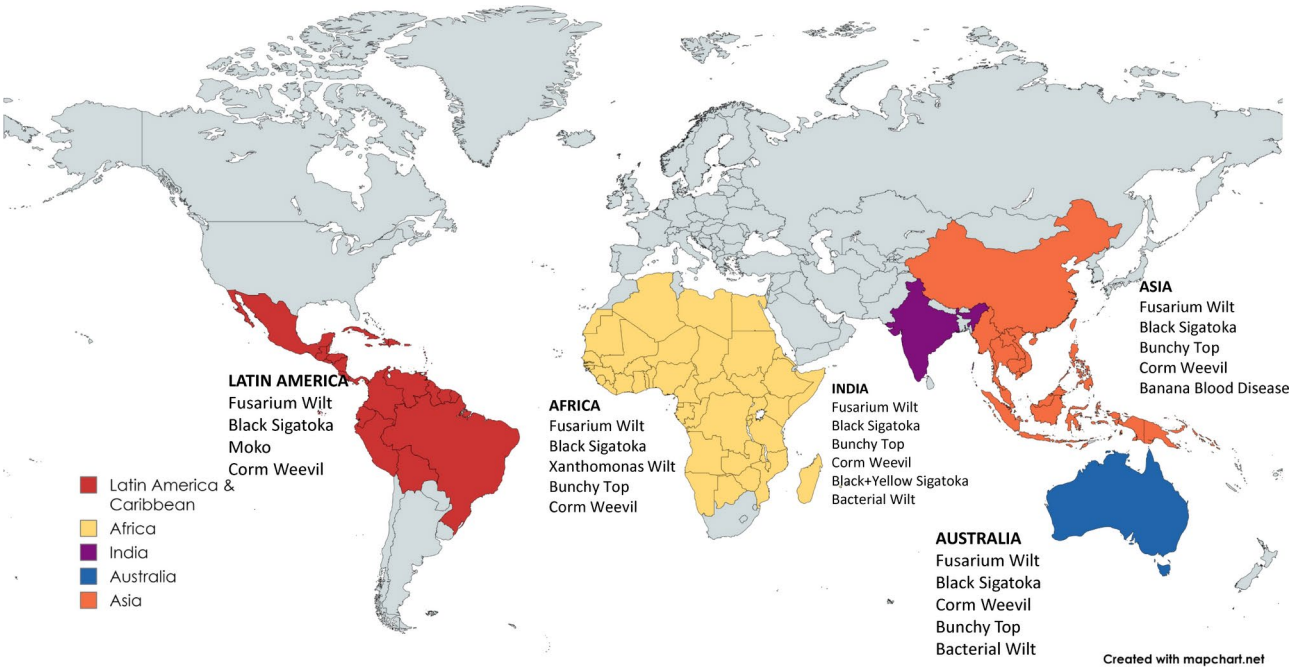

Fig. 4. Regional dataset and model development distribution.

Fig. 5. Annotations of aerial and ground level images. (**a**) Annotation of BXW-Healthy Field, (**b**) Annotation of FW-Healthy Field, (**c**) Annotation of BXW infected banana bunch, (**d**) Annotation of FW Whole Plant, (**e**) Annotation of Black Sigatoka Infected Leaf, (**f**) Annotation of Transversal Cut of Moko Infected Bunch, (**g**) Annotation of Corm affected by Corm Weevil, (**h**) Annotation of Banana Blood Disease in rachis.

Data augmentation

Class imbalance is a notable obstacle in agricultural deep learning (DL) initiatives, as it can cause models to favor the majority class (often healthy plants) and struggle with recognizing less prevalent disease classes[50]. This issue is acutely felt in datasets where healthy crop instances outnumber those with diseased instances[51]. To address this challenge and enrich the dataset with a more balanced representation of both healthy and diseased plants, we employed a strategic data augmentation (DA) approach[52].

We employed six data augmentation techniques, applied randomly, to generate additional training images from the existing ones, thus enriching the dataset with a more diverse array of examples from the minority class (diseased plants). These techniques included:

(i) Image scale variation: Images were scaled to appear closer or further away
(ii) Image rotation: Images were randomly rotated to set number of degrees (between 0 and 60) to the left or right.
(iii) Image translation: Images were shifted along the horizontal and vertical axis, simulating slight camera movements.
(iv) Image flipping: Images were flipped over their vertical axis, creating a mirror effect.
(v) Pixel-brightness variation: Pixel brightness was adjusted by multiplying with a random number, resulting in darker or lighter images.
(vi) Noise addition: Random Gaussian noise or Gaussian blur was added to the images.

Explainable artificial intelligence (XAI) and Grad-CAM

Explainable Artificial Intelligence (XAI), a branch of Machine Learning, that aims to make AI systems transparent and trustworthy[57,58,75]. XAI utilizes ethical principles to unveil the inner workings of these systems.

To understand model decisions, we employed Gradient-weighted Class Activation Mapping (Grad-CAM), an XAI method localizing neuronal activity of a Convolutional Neural Network (CNN). This technique utilizes the gradients of its target class gradients to create a visual map highlighting focus regions for class prediction[58,59]. Grad-CAM, known for its high interpretability and faithfulness to the original model[76], has been chosen for its performance in other fields[61,62,68–72], as the XAI method to explain our models' decisions in this research.

Model training

Partitioning the dataset is crucial in deep learning tasks to prevent overfitting, underfitting, or poor generalization. For our disease detection models on both aerial and ground-level platforms, we adopted an 80/10/10 ratio for training, validation, and testing datasets, respectively. This distribution was consistently applied across all regional datasets, ensuring that the total number of images for each region, as detailed in Tables 1 and 2 and Supplementary Tables 1–4, were divided according to this structure. Since each region's disease profile differs, each regional model is trained on region-specific datasets. To maintain balanced class representation within each set, we employed random selection and distribution across all classes. Due to the complexity of some datasets, all models were trained for 200 epochs using a batch size of 1.

Performance metrics

Loss function

This research evaluated various loss functions to assess model performance. These include Classification Loss (misclassifications), IoU/Localization Loss (bounding box overlap), Dual Focal Loss (class imbalance), Objectness Loss (likelihood of objects in bounding boxes), and Box Loss (bounding box precision)[39,60,61].

Mean average precision (mAP) score

The mean Average Precision (mAP) score is a widely used metric to evaluate a model's ability to accurately and reliably detect objects across multiple categories. It is calculated by averaging the Average Precision (AP) for each object class, providing a comprehensive assessment of detection performance[39,60]. For this project, mAP@0.5 was selected as the baseline configuration, where the Intersection over Union (IoU) threshold is set to 0.5. IoU measures the overlap between the predicted bounding box and the ground truth, with values greater than or equal to 0.5 being considered as correct predictions. This threshold, often referred to as mAP@0.5, represents fair and accurate detection and is commonly treated as a true positive. The decision to use mAP@0.5 was primarily guided by its widespread adoption as a standard benchmark for evaluating object detection models[62,63]. Its clear and easily interpretable results make it a reliable choice for facilitating comparisons with other studies or models, particularly in agricultural and benchmarking projects involving object detection[64]. While stricter IoU thresholds, such as mAP@0.75 or mAP@0.95, can also be considered, these impose stricter criteria for detection accuracy and are generally applied in scenarios requiring highly precise localization.

Precision, recall and F1 score

Precision measures the proportion of correct positive predictions, and recall indicates the proportion of actual positives correctly identified. The F1 score balances precision and recall into a single metric. High F1 scores reflect effective performance. Relevant formulas are shown in Eqs. (1)–(4) [29,39,60,65,66].

$$Precision = \frac{True\ Positives}{False\ Positives + True\ Positives} \tag{1}$$

$$Recall = \frac{True\ Positives}{False\ Negatives + True\ Positives} \tag{2}$$

$$mAP = \frac{1}{number\ of\ classes} \sum_{K=1}^{K=number\ of\ classes} AP_K \tag{3}$$

$$f1\ score = \frac{2 \times precision \times recall}{recall + precision} \tag{4}$$

Deployment and testing of the ground level models in the AI App

The developed ground level disease detection models have been integrated into the latest version of the TUMAINI AI app for Android and iOS smartphones[67]. This flagship application in agricultural innovation is renowned for its ability to accurately identify, classify, and map diseases in banana crops, empowering farmers with improved disease management and crop health monitoring. While TUMAINI is not currently used for collecting or annotating data, it focuses exclusively on assessing plant health. However, future enhancements may enable data capture through the app, which could be leveraged to improve the learning process of the models, further enhancing its capabilities.

For the integration process, we prioritize user experience by adhering to UsableAI and UsefullAI principles. This focus ensures the creation of a seamless and intuitive user interface using the Flutter dynamic UI framework. The resulting cross-platform interface operates smoothly across various devices, guaranteeing a consistent and high-quality user experience.

Following UI development, a Flask API was implemented to connect smartphone image inputs with the backend server. When a user captures a photo or selects an image, it is sent through the API where it is resized and converted into an array format. The server, utilizing PyTorch, then loads the specific model based on the selected plant part and region. Disease prediction is performed and the predicted bounding box dimensions, confidence level, and disease class. These results are then displayed within the app, as detailed in Fig. 6.

To evaluate model effectiveness, comprehensive testing was conducted using a specialized dataset of unseen images from known disease hotspots. This testing dataset comprised 50 images for each disease, encompassing various plant parts (corm, rachis, leaf, cut fruit, whole plant, pseudostem, and bunch) across all study regions. In total 4650 images were tested with the app. This rigorous testing ensures that our models are robust and reliable in identifying and classifying diseases in diverse real-world agricultural settings.

Software and hardware systems used in this study

The study leveraged Python 3.9 as the primary programming language for both algorithm development and data manipulation. To expedite model training, we employed a transfer-learning approach, utilizing pre-trained models from the COCO (Common Objects in Context) dataset[46]. The Faster-RCNN architecture was integrated via the TensorFlow object-detection API zoo with support from Falcon CV 2.0[47]. Additionally, for the YOLOv8, and YOLOv9 architectures, the training process was conducted using the Ultralytics library and PyTorch. This support significantly enhanced the efficiency and scalability of our research efforts. Furthermore, the YOLO-NAS models were developed using the SuperGradients library by Deci-AI[60].

Model training was executed on a remote server equipped with an NVIDIA Tesla M60 graphics card. The server ran the Linux Ubuntu operating system with Python 3.9. Table 4 provides a detailed overview of the hardware and software employed in this study.

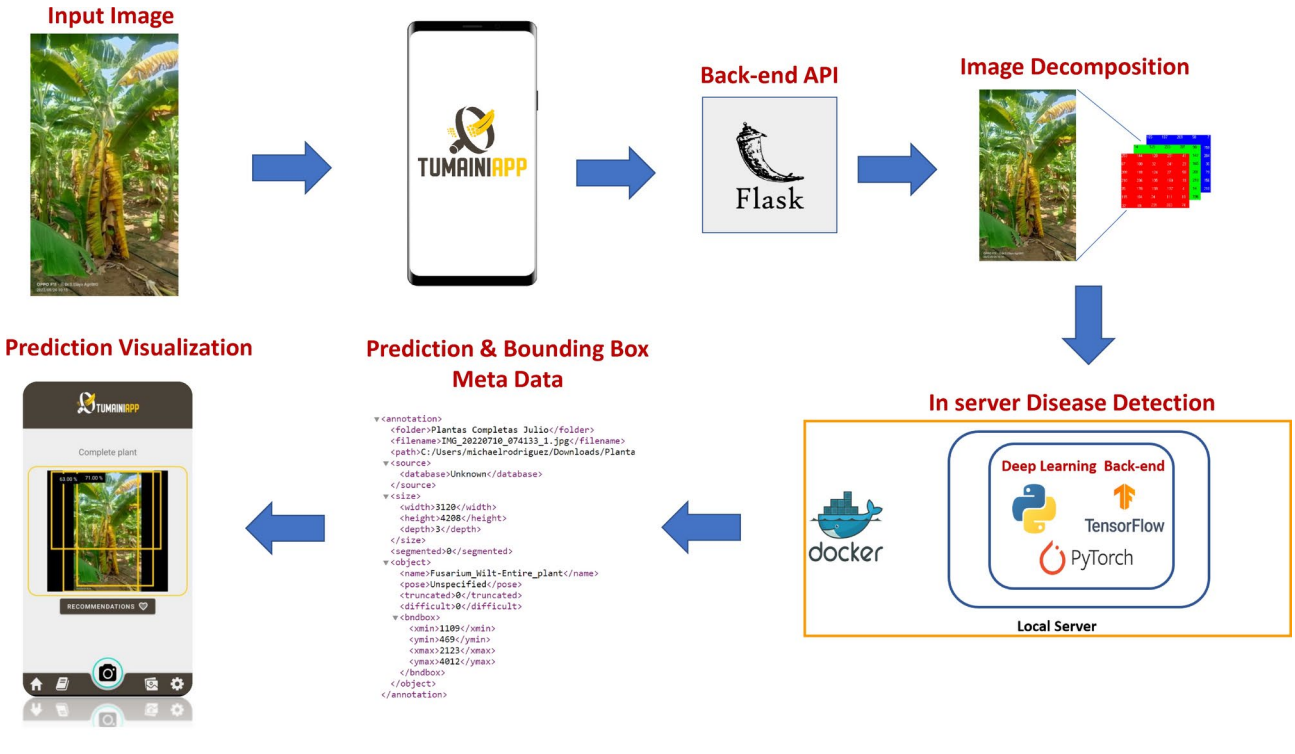

Fig. 6. Description of image detection pipeline using AI APP.

Hardware and software	Specifications
Image acquisition hardware	
Quadcopter UAV	3DR Solo
Quadcopter UAV	Phantom 4 pro
RGB Cameras	Sony Qx1 Hasselblad L1D-20c camera with a 20MP 1″ CMOS sensor
Image processing software	
Orthomosaic Generation	Agisoft MetaShape
DL Modeling hardware	
RAM Memory	128 GB
Processor	Intel Xeon E5-2667 v4 @ 3.20 GHz × 16
GPU	NVIDIA Tesla M60
DL modeling software	
OS	Ubuntu Linux
Programming language	Python 3.9
Labelling software	LabelImg
Deep learning libraries	FalconCV with TensorFlow 2.0 and TensorFlow object detection API PyTorch 1.12.1 with CUDA 11.6, SuperGradients 3.1.3, Ultralytics 8.0.181, Ultralytics 8.1.27, and Ultralytics 8.1.42

Table 4. Hardware and software used in this study.

Type	Images collected	Whole annotations before data augmentation			Whole annotations after data augmentation		
UAV-RGB	6854	Healthy	Xanthomonas Wilt	Fusarium Wilt	Healthy	Xanthomonas Wilt	Fusarium Wilt
		14,238	1523	2041	14,238	4436	4874
Class proportions		80%	9%	11%	60%	19%	21%

Table 5. Aerial platform annotations before and after data augmentation.

Results

Dataset collection and augmentation

Banana pest and disease prevalence is influenced by various environmental factors (e.g., temperature, humidity, rainfall), the specific type of banana, seasonality, and nutritional status. In addition, the distribution of banana diseases is region-specific. For instance, Xanthomonas wilt is primarily concentrated in Africa, while Banana Blood Disease is only prevalent in Southeast Asia[68]. In-depth knowledge of these factors is crucial when developing AI-powered tools for the accurate detection of a biotic constraint and for the subsequent provision of management recommendations. Accurate and reliable image collection from disease hotspots, along with precise labeling of those images, becomes crucial for such efforts. To address this need, we built a comprehensive global, multiplatform solution. Through our CGIAR network, we gathered a substantial image dataset of major banana diseases from various disease hotspots. This data incorporates images captured utilizing both UAVs and ground-level cameras.

This study utilized the extensive collection of banana disease datasets from our Alliance Bioversity-CIAT/CGIAR network[29] supplemented by additional images gathered by banana experts over the past couple of years. The dataset comprises two main categories: 34,800 expertly vetted ground-level images and 6,854 aerial images. The ground-level images comprised a total of 70,263 annotations, while the RGB UAV dataset contained approximately 23,584 annotations as seen in Tables 1 and 2. The regional distribution is detailed in Supplementary Tables 1–4, with 9,99 images from Africa, 4981 from Asia, 9070 from Latin America, and 4101 from India. No images were collected from the Australian continent; however, images from other continents were utilized to develop models that account for the diseases present in this region.

The class distribution within the dataset reflects a typical challenge in agricultural image analysis—class imbalance with healthy plants (82%) being more frequent than diseased plants (10%) infected with Fusarium wilt or Xanthomonas wilt (8%). To mitigate this imbalance and enhance model performance, we employed data augmentation techniques to increase the representation of minority classes. Unlike other studies that utilize partially annotated aerial images[39], our approach ensures complete annotation of each stem in the aerial image dataset.

By randomly selecting and applying two augmentation techniques to each annotation of BXW and FW-infected plants, we were able to increase the representation of minority classes. This resulted in an additional 2913 and 2833 annotations for BXW and FW plants, respectively. Consequently, the distribution of healthy to diseased stem annotations in the RGB dataset was adjusted to a more balanced ratio of 60% healthy, 19% BXW, and 21% FW. Table 5 compares the distributions of the original and augmented datasets.

Evaluation of models for multiplatform disease detection

Ground level platform model selection

We evaluated three different deep learning architectures for ground-level plant disease detection: YOLOv8, YOLO-NAS (single-stage), and Faster-RCNN (two-stage). YOLOv8 and YOLO-NAS have demonstrated positive performance outcomes for their single-stage detection capabilities and real-time processing efficiency[69,70]. Additionally, for two-stage architectures, Faster-RCNN has proved its effectiveness in similar previous studies involving aerial imagery and agricultural deep learning applications[21,48,71–73]. This architecture has consistently shown robust performance, making it a reliable choice for our needs in detailed and precise object detection within agricultural contexts. The models were trained on images captured in the Africa region, focusing on both whole plant and pseudostem annotations[42,79].

Supplementary Tables 5 and 6 offer a comparison of the model's performance for the whole plant and pseudostem annotations. YOLOv8 model demonstrated a robust performance across all categories, by achieving an F1-score of 0.93 for Healthy plants with impressive precision and recall rates, ensuring reliable detection. The model excels in identifying Xanthomonas Wilt with an F1-score of 0.85 indicating its effective detection in a challenging disease category. It continues this trend with Fusarium Wilt and Bunchy Top Virus, reaching F1-scores of 0.86 and 0.90, respectively. The high precision and recall values support its strong performance in these categories. Notably, YOLOv8 achieves an overall mAP@0.5 of 0.91 for whole plant, reflecting its excellent object detection capabilities across different disease conditions. Similarly, in the Pseudostem Annotations, YOLOv8's performance is exemplary. The model secures a F1-score of 0.99 for Healthy, Xanthomonas Wilt, and Fusarium Wilt classifications, showcasing nearly perfect precision and recall. This level of accuracy is highly positive and necessary for precise disease detection. Finally, the mAP@0.5 of 0.99 further verifies its superior detection and classification efficacy compared to the other models.

Supplementary Figs. 1–7 also provide a visual comparison of the model's performance. For the full plant model, YOLO-NAS struggled to accurately detect all the disease categories. Specifically, it missed BBTV infected plants (Supplementary Figs. 1 and 2) and incorrectly identified Xanthomonas wilt infected plant. Faster-RCNN, on the other hand, while exhibiting a better performance than YOLO-NAS, often generated multiple bounding boxes for a single object, suggesting over-detections. Notably, YOLOv8 successfully detected all the ground truth annotations for both whole plant and pseudostem classes, with its prediction boxes closely aligning with the actual objects. For the pseudostem class, the performance was more balanced across all models, with detections being correct and high confidence for all classes.

Overall, the YOLOv8 model emerged as the superior choice for deployment due to its exceptional performance across various metrics. It consistently achieved high scores in individual precision, recall, F1-score, and mAP@0.5 for all classes across plant parts. This balanced performance ensures its ability to identify most disease instances correctly while minimizing false positives, which is crucial for effective disease enhancement and increased agricultural productivity.

Loss function analysis for aerial platform

The analysis of the Faster-RCNN model training over 200 epochs revealed a detailed understanding of its effectiveness in object detection (supplementary Fig. 8). The Region Proposal Network's (RPN) objectness loss, decreased sharply before plateauing. This indicates the model's rapid learning to identify potential objects early in training and maintaining that capability. Similarly, the RPN localization loss also showed a gradual decrease which signifies the model's increasing precision in locating objects. The box classifier's localization and classification losses also showed consistent declines, highlighting ongoing enhancements in the model's ability to pinpoint and correctly classify objects within the bounding boxes. Overall, these results demonstrate Faster-RCNN's effectiveness in mastering both crucial aspects of object detection.

The YOLO-NAS model's total loss exhibited considerable variability during training, characterized by occasional spikes and an overall average level. Which indicates high variability and spikes in the classification Loss indicate inconsistencies in distinguishing between different object classes. In contrast, the YOLOv8 model, analyzed through various metrics over 200 epochs, displayed a different pattern in its learning dynamics. The Total Loss for the YOLOv8 model initially decreased sharply and then stabilized, indicating a learning plateau, suggesting that the model has learned the diminishing returns from further training on the same dataset. Similar trends were observed in the classification loss and dual focal loss plots, showing significant drops followed by stabilization. The IOU Loss, indicating the model's accuracy in bounding box predictions, showed minimal fluctuations, signifying consistent performance in accurately localizing objects accurately throughout the training.

Finally, the YOLOv9 model displayed exceptional learning efficiency during training and validation performance over 200 epochs. The total Loss exhibited a sharp decline early in training, followed by stabilization at a low level. Also, the steep initial decrease followed by a plateau in the IOU Loss and Dual Focal Loss graphs reflected the model's rapid learning of spatial relationships between objects and its subsequent consistent localization performance throughout training. The Classification Loss also displayed a steep drop early in training and remained consistently low throughout.

Overall, this learning pattern demonstrated that the YOLOv9 model achieved a more stable learning curve and effectively exhibited better generalization capabilities compared to YOLOv8. While YOLO-NAS and YOLOv8, showed gradual improvement in detection capabilities amidst training challenges, it might require further optimization to refine their performance, whereas Faster-RCNN and YOLOv9 exhibited a more consistent and stable learning curve, making it potentially more reliable choice in practical object detection scenarios.

Classes	Aerial Images			
	mAP@0.5			
	Yolo-NAS	YOLO-v8	YOLO-v9	Faster-Rcnn
Healthy	0.36	0.73	0.8	0.69
Fusarium Wilt	0.35	0.65	0.68	0.7
Xanthomonas Wilt	0.34	0.79	0.77	0.71
TOTAL AVERAGE	0.35	0.72	0.75	0.7

Table 6. mAP@0.5 performance for aerial platform models.

Model	Africa						
	mAP@0.5						
Classes	Rachis	Cut fruit	Whole plant	Leaf	Bunch	Pseudostem	Corm
Healthy	0.98	0.92	0.86	0.69	0.96	0.99	0.98
Xanthomonas Wilt	–	0.92	0.92	0.85	0.99	0.99	–
Fusarium Wilt	–	–	0.93	0.75	–	0.99	–
Bunchy Top Disease	–	–	0.87	–	–	–	–
Black Sigatoka	–	–	–	0.80	–	–	–
Moko	–	–	–	–	–	–	–
Banana Blood Disease	–	–	–	–	–	–	–
Black Sigatoka + Yellow Sigatoka	–	–	–	–	–	–	–
Bacterial Wilt	–	–	–	–	–	–	–
Corm Weevil	–	–	–	–		–	0.99
Total Average	0.98	0.92	0.89	0.80	0.98	0.99	0.99

Table 7. mAP metric score per class, at ground level, in the Africa Region (IOU = 0.5, Conf = 0.5).

Loss function analysis for ground level platform

The post training analysis of 35 YOLOv8 models, emphasizing efficiency, adaptability, and stability for ground-level plant disease detection, is presented in supplementary Figs. 9–13. All trained models exhibited a rapid initial decline in loss, signifying efficient learning and adaptation to the dataset. This consistent decline in model loss throughout training further validates the effectiveness of the procedure.

However, some classes, particularly the leaf class across all regions and whole plants in Africa, Asia, and India, exhibited an anomaly. In these scenarios, the dual focal validation loss initially decreased but began increasing after 100 epochs. Despite this anomaly, all models exhibited a consistent and steady decline in loss up to a certain point, indicating a positive stability in their learning process.

mAP score analysis for aerial platform

The mAP scores for disease detection on the aerial platform is represented in Table 6. YOLOv9 achieved the highest mAP score (0.8) for identifying healthy plants, followed by YOLOv8 (0.73), and Faster-RCNN (0.69), and YOLO-NAS (0.36). For Fusarium Wilt, Faster-RCNN led with a mAP of 0.7, slightly surpassing YOLOv9 (0.68) and YOLOv8 (0.65), while Yolo-NAS displayed lower performance (0.35). YOLOv8 excelled all other models in detecting Xanthomonas Wilt, achieving an mAP of 0.79, followed closely by YOLOv9 (0.77) and Faster-RCNN (0.71), with YOLO-NAS again showing the lowest performance (0.34).

The aggregate scores across all classes highlight YOLOv9 as the overall best performer with a combined mAP score of 0.75, indicating superior detection accuracy. YOLOv8 and Faster-RCNN also delivered strong results of 0.72 and 0.7, respectively. However, YOLO-NAS, requires further improvement as its total score was 0.35. This comparative analysis suggests that YOLOv9 might be the most effective model for aerial plant health surveillance, offering higher precision in identifying various plant conditions compared to other models tested.

mAP score analysis for ground level platform

Tables 7, 8, 9, 10 and 11 present the mAP scores of various YOLOv8 models, segmented by plant parts across different regions. In the Africa region, the mAP scores range from 80 to 99%, indicating strong performance across most plant parts except for leaves (80%) and whole plants (89%). The lowest mAP scores were observed for the leaf category in Fusarium Wilt and Healthy classes, and for the plant category in Healthy and Bunchy Top classes.

Similar performance patterns were observed in Latin America, with 86% accuracy for leaf and 79% for whole plant classification. Across other regions including India, Asia, and Australia, whole plant models achieved scores ranging from 86 to 91%, while leaf models ranged from 75 to 79%. Conversely, the models detecting

Model	Latin America						
	mAP@0.5						
Classes	Rachis	Cut fruit	Whole plant	Leaf	Bunch	Pseudostem	Corm
Healthy	0.99	0.9	0.83	0.65	0.91	0.99	0.985
Xanthomonas Wilt	–	–	–	–	–	–	–
Fusarium Wilt	–	–	0.87	0.7	–	0.98	–
Bunchy Top Virus	–	–	–	–	–	–	–
Black Sigatoka	–	–	–	0.9	–	–	–
Moko	0.99	0.94	0.88	0.89	0.96	0.73	–
Banana Blood Disease	–	–	–	–	–	–	–
Black Sigatoka + Yellow Sigatoka	–	–	–	–	–	–	–
Bacterial Wilt	–	–	–	–	–	–	–
Corm Weevil	–	–	–	–	–	–	0.99
Total Average	0.99	0.92	0.86	0.785	0.935	0.9	0.99

Table 8. mAP metric score per class, at ground level, in the Latin American Region (IOU = 0.5, Conf = 0.5).

Model	India						
	mAP@0.5						
Classes	Rachis	Cut fruit	Whole plant	Leaf	Bunch	Pseudostem	Corm
Healthy	0.99	0.91	0.89	0.6	0.91	0.99	0.985
Xanthomonas Wilt	–	–	–	–	–	–	–
Fusarium Wilt	–	–	0.91	0.92	–	0.99	–
Bunchy Top Virus	–	–	0.85	–	–	–	–
Black Sigatoka	–	–	–	–	–	–	–
Moko	–	–	–	–	–	–	–
Banana Blood Disease	–	–	–	–	–	–	–
Black Sigatoka + Yellow Sigatoka	–	–	–	0.81	–	–	–
Bacterial Wilt	0.97	0.95	0.93	0.69	0.96	0.99	–
Corm Weevil	–	–	–	–	–	–	0.99
Total Average	0.98	0.93	0.895	0.755	0.935	0.99	0.99

Table 9. mAP metric score per class, at ground level, in the India Region (IOU = 0.5, Conf = 0.5).

Model	Asia						
	mAP@0.5						
Classes	Rachis	Cut Fruit	Whole Plant	Leaf	Bunch	Pseudostem	Corm
Healthy	0.99	0.9	0.85	0.71	0.94	0.99	0.99
Xanthomonas Wilt	–	–	–	–	–	–	–
Fusarium Wilt	–	–	0.87	0.7	–	0.99	–
Bunchy Top Virus	–	–	0.8	–	–	–	–
Black Sigatoka	–	–	–	0.9	–	–	–
Moko	–	–	–	–	–	–	–
Banana Blood Disease	0.97	0.89	0.9	0.69	0.96	0.99	–
Black Sigatoka + Yellow Sigatoka	–	–	–	–	–	–	–
Bacterial Wilt	–	–	–	–	–	–	–
Corm Weevil	–	–	–	–	–	–	0.99
Total Average	0.98	0.895	0.855	0.75	0.95	0.99	0.99

Table 10. mAP metric score per class, at ground level, in the Asian Region (IOU = 0.5, Conf = 0.5).

Model	Australia						
	mAP@0.5						
Classes	Rachis	Cut Fruit	Whole Plant	Leaf	Bunch	Pseudostem	Corm
Healthy	0.98	0.94	0.9	0.69	0.91	0.99	0.99
Xanthomonas Wilt	–	–	–	–	–	–	–
Fusarium Wilt	–	–	0.86	0.72	–	0.99	–
Bunchy Top Virus	–	–	0.95	–	–	–	–
Black Sigatoka	–	–	–	0.86	–	–	–
Moko	–	–	–	–	–	–	–
Banana Blood Disease	–	–	–	–	–	–	–
Black Sigatoka + Yellow Sigatoka	–	–	–	–	–	–	–
Bacterial Wilt	0.97	0.95	0.91	0.89	0.96	0.99	–
Corm Weevil	–	–	–	–	–	–	0.99
Total Average	0.975	0.945	0.905	0.79	0.935	0.99	0.99

Table 11. mAP metric score per class, at ground level, in the Australian Region (IOU = 0.5, Conf = 0.5).

bunch, corm, and rachis continue to perform exceptionally well, with mAP scores ranging from 90 to 99% across these regions. This highlights the model's strengths and potential reliability in detecting less variable disease conditions.

YOLOv8 models demonstrated varying performance across different plant parts. While achieving robustness in some cases, the differences in loss patterns and mAP scores indicated potential challenges for specific plant parts and datasets, highlighting the need for tuning the model tailored for specific adjustments.

Confusion matrix analysis of YOLO models for aerial platform

In our study, confusion matrices served as a pivotal tool for assessing the performance of various YOLO model variants. They revealed instances where model performance suffered due to class complexity, providing insights into areas prone to errors for targeted improvements.

As seen in supplementary Fig. 14, Faster-RCNN model achieved moderate accuracy of 72% for healthy plants, however, exhibited substantial inaccuracies, including 25% undetected healthy plants and 41% high false positives. The detection rates for Xanthomonas Wilt and Fusarium Wilt stand at 73% and 65%, respectively, but plagued by false negatives and false positives. This pattern suggests the need for improvements in the model, potentially through balanced training datasets or refined classification algorithms.

The YOLO-NAS model achieved 79% accuracy in identifying healthy plants but displayed a high rate of false positives across all classes. Disease detection for Xanthomonas Wilt and Fusarium Wilt were low with accuracies of 38% and 40%, respectively. However, the model struggled with high rates of misclassifications and undetected cases for these diseases. This performance of the YOLO-NAS model highlights the need for further tuning and optimization, particularly on enhancing its specificity and reducing false positives detections.

In contrast, the YOLOv8 model, effectively recognized some certain plant conditions, but faced considerable challenges with misclassifications and undetected cases. It successfully identified 64% of healthy plant instances but failed to detect 35% of such conditions, indicating a high false negative rate. The model's performance on Xanthomonas Wilt showed a better accuracy of 79%, yet it still missed 19% of these cases. Fusarium Wilt detection was accurate in 69% of instances, with 26% of cases going undetected. The model exhibited low false positives for healthy plants and Xanthomonas Wilt but struggled with Fusarium Wilt, underscoring the need for further tuning to enhance reliability and reduce false negatives.

Finally, YOLOv9 exhibited robust detection capabilities with high true positive rates of 73% for healthy plants and Xanthomonas Wilt, and 70% for Fusarium Wilt. Nonetheless, it also displayed significant false negative rates across all conditions (21–23%) and particularly high false positive rates for Xanthomonas Wilt (24%). Notably, YOLOv9 produced very few extra detections, indicating a conservative detection threshold that avoids spurious results but might benefit from adjustments to improve sensitivity and reduce misclassifications.

Confusion matrix analysis of YOLO models for ground level platform

Our analysis of YOLO model performance at ground level revealed both strengths and weaknesses across various regions in Africa, Latin America, Asia, India, and Australia (see Supplementary Figs. 15–19).

In Africa, the models exhibited high accuracy (90%) for Cut Fruit and Pseudostem, particularly in detecting Xanthomonas Wilt. However, models faced challenges with Leaf and Whole Plant categories, particularly for Xanthomonas and Fusarium Wilt, with up to 26% undetected cases.

In Latin America, the confusion matrices displayed high accuracy for specific diseases such as Moko disease, where it identifies 85% of the cases in Cut Fruit and an impressive 98% in Bunch. However, it exhibited weaknesses in consistently recognizing healthy conditions, with undetected rates of 22% for healthy Cut Fruit and 7% for Rachis. Leaf assessments also struggled, achieving 74% accuracy with 26% undetected healthy leaves.

In Asia, the models showed a strong capability to detect diseases with high accuracy rates for Banana Blood disease (82%) and Black Sigatoka (77%) in leaves. However, the model struggled to accurately confirm

the absence of disease, misclassifying 23% of healthy leaves as undetected. While achieving 82% accuracy in detecting Banana Blood Disease, 17% of cases remained undetected.

In India, the model demonstrated a balanced performance across various plant parts with high accuracy in detecting symptoms of specific disease like Bacterial Wilt (85% for Cut Fruit and 95% for Bunch). However, the model exhibited higher rates of undetected healthy plants across leaf and whole plant categories.

Similarly, in Australia, the model performed exceptionally well in detecting specific diseases, reaching 99% for diseases like Fusarium Wilt in the Whole Plant category. However, it exhibited a recurring issue with detecting healthy conditions, where a considerable percentage of healthy plants were either misclassified or undetected. For example, in the Corm and Bunch assessments, while the detection rates for diseases were above 90%, the undetected rates for healthy conditions ranged from 7 to 10%.

Evaluation of YOLO models using precision and recall metrics for aerial platform

The performance comparison of four distinct object detection models—YOLO-NAS, YOLOv8, YOLOv9, and Faster-RCNN—for plant health conditions is presented in Table 12. The table provides a comprehensive overview of model performance across Healthy, Xanthomonas Wilt, and Fusarium Wilt conditions, using precision, recall, and F1-Scores. Notably, YOLO-NAS underperformed across all conditions, with low scores (precision, recall, and F1-Score all below 0.10). In contrast, YOLOv8 and Faster-RCNN demonstrated robust performance in detecting healthy plants, achieving precision and F1-Scores above 0.74. Faster-RCNN had a higher recall for healthy plants, while YOLOv9 emerged as the top performer in the Healthy category with a precision of 0.83 and the highest F1-Score of 0.79.

For Xanthomonas Wilt, YOLOv8 demonstrated the highest recall and F1-Score among the models, with strong detection reliability. YOLOv9 showcased superior precision for Xanthomonas Wilt, but its lower recall affected its overall F1-Score compared to YOLOv8 and finally Faster-RCNN remained consistent, across all three metrics with a slightly lower performance. In the Fusarium Wilt category, YOLOv9 obtained precision and recall scores of 0.63 and 0.64 respectively while YOLOv9 again led in precision, but its recall significantly dropped, which balanced its overall F1-Score to 0.66. The best performing model in this scenario was Faster-RCNN which exhibited more consistent metric outcomes obtaining a f1 score metric 0.67.

Evaluation of YOLOv8 models using precision and recall metrics for ground level platform

The performance of YOLOv8 models were analyzed across different plant parts (Rachis, Cut Fruit, Whole Plant, Leaf, Bunch, Pseudostem, and Corm) and regions (Africa, Latin America, South East Asia, India, and Australia) using precision, recall, and F1 scores for ground level platform (Tables 13, 14, 15, 16 and 17).

Overall, the models exhibited high performance in categories like Rachis, Bunch, Pseudostem, and Corm across all regions during the training and testing phases, achieving F1 scores exceeding 0.92, which makes the models accurate and reliable for these specific plant parts (Table 13, 14, 15, 16 and Table 17). However, the Leaf category displayed lower performance metrics compared to the other parts with values ranging between 0.76 and 0.85.

The evaluated YOLOv8 models demonstrated varying performance across plant parts. While achieving high accuracy in certain areas, consistent struggles arose in leaf categories across all regions. This indicates that despite the positive results, further model enhancements including improved data collection methods, advanced augmentation techniques, and a broader inclusion of diverse symptomatology in the training stages will continue to help to improve the models' generalizability and real-world agricultural applicability.

Model deployment and testing in AI powered app

The Tumaini App, developed in 2019 by the Alliance of Bioversity International and CIAT[77], is an AI-powered mobile application for banana disease detection in which users can upload or capture images for real-time analysis. The app was evaluated using unseen real-field images from various disease hotspots—Africa, Latin America, India, Southeast Asia, and Australia. The results presented in Supplementary Tables 7–11 demonstrate high accuracy and confidence in detecting plant diseases and healthy conditions, although variations in misdetection rates indicate areas for fine-tuning.

In Africa, the models exhibited strong performance in detecting Black Sigatoka and Xanthomonas Wilt in leaves, with perfect accuracy and high average confidence scores exceeding 80%. While Whole Plant accuracy dropped to 80% with an 87% confidence level, the model encountered difficulties with classifying complex symptoms across entire plants.

Similar patterns were observed in Latin America, with high accuracy for Fusarium Wilt in leaves and Moko in bunches, both nearing perfect accuracies. However, the accuracy dropped to 74% with a significantly lower

	Healthy			Xanthomonas Wilt			Fusarium Wilt		
Model	Precision	Recall	F1-Score	Precision	Recall	F1-Score	Precision	Recall	F1-Score
YOLO-NAS	0.11	0.08	0.09	0.07	0.05	0.06	0.11	0.08	0.09
YOLOv8	0.76	0.72	0.74	0.80	0.77	0.78	0.63	0.64	0.63
YOLOv9	0.83	0.75	0.79	0.86	0.65	0.74	0.83	0.55	0.66
Faster-Rcnn	0.76	0.78	0.77	0.74	0.72	0.73	0.70	0.64	0.67

Table 12. Precision, recall and F1-score for aerial models.

Model	Africa																				
	Rachis			Cut fruit			Whole plant			Leaf			Bunch			Pseudostem			Corm		
Classes	Precision	Recall	F1 Score	Precision	Recall	F1 Score	Precision	Recall	F1 Score	Precision	Recall	F1 Score	Precision	Recall	F1 Score	Precision	Recall	F1 Score	Precision	Recall	F1 Score
Train	0.99	0.99	0.99	0.94	0.90	0.92	0.96	0.89	0.92	0.86	0.72	0.78	0.98	0.98	0.98	0.99	0.98	0.98	0.99	0.99	0.99
Test	0.98	0.98	0.98	0.94	0.86	0.90	0.94	0.84	0.89	0.90	0.70	0.79	0.96	0.92	0.94	0.99	0.99	0.99	0.97	0.98	0.97

Table 13. Precision, recall and F1-score for ground level models in Africa.

confidence of 47% when detecting Moko in Pseudostems, indicating that the model encountered challenges, with misclassification.

India reflected high accuracy across most categories, with perfect scores in detecting Bacterial Wilt symptoms in Cut Fruit and Fusarium Wilt in leaves. However, Bacterial Wilts symptoms in Pseudostem presented a lower accuracy of 78% and a low confidence score of 47%, mirroring the challenges seen with Moko in Latin America.

For Southeast Asia, the detection accuracies were high across all categories with particularly strong performance in detecting Banana Blood Disease and Black Sigatoka in leaves. Yet, Whole Plant detection showed slightly reduced accuracy and confidence, especially for healthy conditions and Banana Blood Disease, indicate potential difficulties in general plant condition assessments.

Finally, Australia boasted high accuracy across the board, notably in detecting Bunchy Top Virus in Whole Plants and Bacterial Wilt in Cut Fruit. However, the model exhibited slightly lower accuracy in classifying symptoms of Bacterial Wilts in Pseudostems and Fusarium Wilt in Whole Plants, achieving around 92% accuracy with reduced confidence levels compared to other conditions.

While the models exhibited high efficacy in identifying specific diseases, recurring challenges arose in accurately detecting broader categories like healthy conditions in Whole Plants and specific diseases in Pseudostems. These results emphasize the crucial need for optimization, especially in accurately identifying healthy plants and disease-specific symptoms across different plant parts.

App features

Step by step disease detection using HILAI

The TumainiAPP employs a HILAI-based step-by-step algorithm tailored to specific regions and initial symptoms[78,85]. This approach illustrated in Supplementary Figs. 20–24, enhances disease management strategies in banana cultivation. Additionally, the combination of HILAI and effective UX design allows users for model refinement, confirming or denying the model's predictions and focusing on key symptoms, enhancing accurate detection. Figure 7 illustrates this process in the app.

Database

The Tumaini APP is built upon a georeferenced banana database comprising over 70,000 banana plants gathered between 2015 and 2024. Each entry includes the disease name and latitude/longitude coordinates of the corresponding infected plant. The dataset encompasses information on both healthy plants and those afflicted with various diseases, including Fusarium Wilt, Moko, Xanthomonas Wilt, Banana Bunchy Top Virus, and leaf fungal diseases (Black Sigatoka + Yellow Sigatoka), across 17 countries worldwide. Data was gathered through in-field surveys, analysis of drone imagery, and extraction of metadata from ground-level images captured using smartphones. Table 18 provides a detailed overview of the dataset.

Disease mapping and online platform

The Tumaini APP leverages a PostgreSQL database for efficient data management and retrieval. An online dashboard at tumainiaiapp.org allows users to explore a global map visualizing plant distribution, with functionalities for filtering and sorting. Furthermore, the online dashboard seamlessly integrates with the Tumaini App, allowing users to map banana plants directly from their mobile devices using GPS coordinates or manual locations entry. Mapped data seamlessly uploads to the database, enhancing the accessibility and usability of the database.

User profiles and connections between users

Upon registration, users are prompted to select their occupation from three distinct classes: Farmer, National Phytosanitary Protection Organization (NPPO), or researcher. This classification system facilitates tailored access to features and information relevant to each user's professional role. Users can establish partnerships with other platform users, enabling the sharing of mapped plant information and facilitates collaboration among individuals with common interests or objectives. Notably, there is no limit on the number of users that can be added as partners, ensuring scalability and unhindered growth of the platform's collaborative network. This approach fosters a dynamic and inclusive community where users can actively contribute to and benefit from shared insights and collective efforts in monitoring banana plant health. The platform's notification system promptly informs users when their partners map new plants, promoting real-time engagement and collaboration.

Discussion

YOLOv9 for identifying diseases in banana crops from aerial images

In our analysis of aerial images, YOLOv9 showcased superior performance in detecting healthy, fusarium wilt, and Xanthomonas wilt-infected plants. Overall, YOLOv9 ranked highest when comparing metrics such as mAP@0.5 and F1 score. Although YOLOv8 and Faster-RCNN outperformed YOLOv9 in specific scenarios, such as the mAP score for some individual diseases, the overall performance across all classes were similar between Faster-RCNN and YOLOv8 and slightly lower than YOLOv9. YOLO-NAS, on the other hand, struggled to achieve similar performance compared to its competing models obtaining lower scores across all metrics. This behavior is expected, as YOLO-NAS has been proven to be more effective with close-up images and detecting small objects[74] rather than images at large distances such as the drone images used in this study. This analysis highlights the specific strengths and weaknesses of each model. YOLOv9 generally provided the best balance of high precision and satisfactory recall, making it a strong choice for applications requiring nuanced detection capabilities, despite some inconsistencies in specific conditions[36,85].

When considering the deployment of the models, processing and inference times are relevant. While models such as Faster-RCNN provide sufficient performance based on the detection metrics, these architectures face difficulties in terms of inference times due to the complexity of its two-stage architecture[74,75]. Unlike Faster-RCNN's two-stage

Model	Latin America																				
	Rachis			Cut fruit			Whole plant			Leaf			Bunch			Pseudostem			Corm		
Classes	Precision	Recall	F1 Score	Precision	Recall	F1 Score	Precision	Recall	F1 Score	Precision	Recall	F1 Score	Precision	Recall	F1 Score	Precision	Recall	F1 Score	Precision	Recall	F1 Score
Train	0.98	0.98	0.98	0.93	0.86	0.89	0.83	0.79	0.81	0.81	0.71	0.76	0.94	0.92	0.93	0.92	0.87	0.89	0.99	0.99	0.99
Test	0.98	0.97	0.97	0.9	0.94	0.92	0.94	0.74	0.83	0.9	0.67	0.77	0.97	0.98	0.97	0.98	0.81	0.89	0.97	0.98	0.97

Table 14. Precision, recall and F1-Score for ground level models in Latin America.

process, one-stage architectures like YOLOv8 and YOLOv9 can identify objects in a single step, leading to faster inference times[74,75].

The visual performance of each architecture can be observed in supplementary Figs. 20 and 21, which showcase the detection of FW & BXW from the aerial platform across all models. Here, we see similar performances to those described for the ground level models. However, faster-RCNN, utilizing its region proposal network, tends to generate more bounding boxes compared to single stage models. Subsequently YOLO-NAS performs poorly, failing to detect most healthy and infected plants. Finally, YOLOv8 and YOLOv9 achieve accurate detections for all classes.

To understand how each architecture differentiates each class, we employed Explainable AI (XAI) and the GradCAM technique. Figures 8, 9, and 10 exhibit the feature maps for Faster-RCNN, YOLOv8, and YOLOv9. For Faster-RCNN, we observe that the "Healthy" subplot's heatmap primarily shows green and yellow hues around the plant's main leaves. This suggests that these areas play a crucial role in the model's classification of healthy plants. In contrast, the "Xanthomonas Wilt" subplot highlights regions with symptoms like wilting or discolored leaves. Interestingly, areas with dried leaves appear less emphasized. Similarly, the "Fusarium Wilt" subplot highlights areas with yellowing leaves, indicating the model's reliance on leaf color for disease differentiation. These visualizations demonstrate that Faster-RCNN prioritizes specific cues, particularly complete leaves and their color, to differentiate between healthy and diseased plants.

In Fig. 9, the YOLOv8 model prioritizes plant structure. While its heat map for healthy plants is more dispersed, it also incorporates some background features. For Xanthomonas Wilt, the heatmap emphasizes the outermost, dried-out leaves. In contrast, for Fusarium Wilt, it highlights the complete leaf arrangement, particularly focusing on yellow leaves over green ones.

Lastly, YOLOv9's performance is similar to YOLOv8's, with the main difference being a more concentrated focus on the plant's features rather than the background, especially for the healthy class. It is important to note that Fusarium Wilt and Xanthomonas Wilt share similar symptoms despite being caused by different agents. In this study, the differentiation of these classes benefits from the advanced stage of the BXW images, where some plants exhibit significant wilting and reduced foliage. This creates a visual difference between BXW and FW plants, allowing the models to establish a clear classification for all three classes from aerial imagery.

Models such as YOLOv8 and YOLOv9 have gained recognition for their accurate detections and short inference times. These reduced processing times have enabled their applications in video formats. Applications of these YOLO models in video object detection and tracking in in fields like surveillance and agriculture has explored[76–80]. Despite positive advancements in this field, applications in banana crops remain underexplored. We have taken an initial approach by implementing the models developed in this study. Supplementary material 1 shows video footage of the YOLOv9 model detecting sick and healthy plants in a Fusarium infected field in northern Peru. While further testing and validation are required, this initial approach represents a promising first step towards Realtime aerial surveillance for banana crops, exhibiting the potential of these developed models.

Overall, the positive performance of all models, especially YOLOv9, represents a significant advancement in terms of aerial crop surveillance for banana plantations. This cutting-edge model not only enhances disease detection accuracy and speed but also opens new avenues for real-time crop health monitoring and management.

YOLOv8 for identifying diseases in banana crops from ground level images

For the ground level image analysis and disease detection, YOLOv8 was selected as the base architecture for training all 35 models after testing several different architectures for the WholePlant and Pseudostem class. Overall, YOLOv8 exhibits superior performance compared to YOLO-NAS and Faster-RCNN in terms of precision, recall, F1 score and mAP@50. This foundation model has demonstrated high prowess in accurately detecting diseases for all plant parts, this performance is related to several key advantages. Firstly, YOLOv8 is optimized for real-time processing, thanks to its single-stage architecture that allows for rapid detection with minimal latency unlike Faster-RCNN[74]. Secondly, YOLOv8's architectural efficiency is enhanced by the C2f. module, which combines high-level features with contextual information, and a decoupled head architecture that processes objectness, classification, and regression tasks independently.

Different applications such as animal counting[81], identification of wildfire and smoke detection[82], ball and foul tracking in football have also shown similar results[83,84] when comparing these architectures. All of these scenarios have highlighted YOLOV8 for having a higher performance in terms of f1 score and mAP than other methods like Faster-RCNN and YOLO-NAS.

Regardless of its accurate performance, the findings emphasize that while YOLOv8 models achieve high accuracy in several plant parts, performance deficiencies are apparent when dealing with more complex annotations, particularly for leaves and whole plants. During the training process loss functions, particularly for leaf and whole plant classes exhibit variations with the loss values increasing after 100 steps. Regarding other metrics, the results exhibit lower accuracy in detecting leaf diseases for Latin America, Asia, and Australia as well as lower f1 scores when comparing training to testing data in the leaf classes across all regions. These results may be attributed to the increased complexity of these datasets compared to others. Leaf and whole plant annotations often show less variability between classes, as yellowing and wilting are common symptoms for different diseases[70,76]. Issues related to disease detection in these specific plant parts are not unknown. The current model's performance aligns with previous findings which highlight difficulties in disease detection due to the amount of background noise in complete plant images, large size of banana leaves and overlapping of multiple leaves with different health status[29]. Overall, this trend highlights a universal challenge in accurately detecting leaf-specific diseases.

This insight is critical for future model development, underscoring the need for more specific tuning and advanced training techniques to handle higher variability or complexity in datasets. Enhancing the models' ability to detect these challenging categories is essential for improving their utility in precision agriculture, ensuring reliable and accurate disease detection across diverse conditions.

Model	India																				
	Rachis			Cut fruit			Whole plant			Leaf			Bunch			Pseudostem			Corm		
Classes	Precision	Recall	F1 Score	Precision	Recall	F1 Score	Precision	Recall	F1 Score	Precision	Recall	F1 Score	Precision	Recall	F1 Score	Precision	Recall	F1 Score	Precision	Recall	F1 Score
Train	0.98	0.98	0.98	0.92	0.89	0.90	0.88	0.77	0.82	0.81	0.73	0.77	0.94	0.91	0.92	0.92	0.88	0.90	0.99	0.99	0.99
Test	0.98	0.97	0.97	0.9	0.94	0.92	0.96	0.82	0.88	0.8	0.7	0.75	0.97	0.98	0.97	0.98	0.81	0.89	0.97	0.98	0.97

Table 15. Precision, recall and F1-Score for ground level models in India.

Despite the performance gaps identified, particularly in complex annotations, which highlight the necessity for ongoing refinement and specialized training techniques. The practical implications for both the aerial and ground level models are evident across various applications, not only in banana surveillance but also other topics in precision agriculture. Future efforts should focus on addressing these challenges to fully harness the potential of these advanced detection models, ensuring their applicability and reliability in diverse real-world scenarios. This development of these models serves as the AI backbone for the complete surveillance system.

Impact on agriculture and crop surveillance

The AI framework developed in this study demonstrates significant advancements in BXW and FW management through an integrated multiplatform detection pipeline. By combining drone-based aerial analysis with a ground-level AI-powered app, the system provides efficient, scalable, and accurate monitoring of banana diseases across diverse landscapes. Drone image analysis enables rapid coverage of large areas, reducing the time and labor involved in manual inspections, while the ground-level app allows for close-up verification and detailed disease confirmation. This two-tiered approach ensures early detection of diseases, facilitates timely interventions, and minimizes crop loss, significantly enhancing disease management practices.

The integration of Explainable AI (XAI) further enhances the system's transparency and reliability. XAI helps elucidate how the model distinguishes between healthy plants and those affected by Fusarium Wilt and Xanthomonas Wilt, fostering user trust by providing clear and interpretable decision-making processes[85]. Additionally, the use of Human-in-the-Loop AI (HILAI) ensures continuous model improvement through user feedback, reducing false positives and negatives. The app's ability to guide users in identifying symptoms on other plant parts mimics traditional field scouting practices, offering a comprehensive diagnostic approach. Moreover, the mapping feature of the Tumaini App integrates aerial and ground-level data into a unified online platform, enabling real-time monitoring, visualization of healthy and infected plants, and strategic decision-making for disease control.

Overall, the performance of the developed models and systems in this study aligns closely with similar research projects focused on infectious disease detection in plants using deep learning. Numerous studies have applied various machine learning and deep learning approaches to identify diseases in crops. For instance, YOLO architectures have been widely utilized for disease detection in other crops, such as peppers, sugar beet plants, and bananas, achieving accuracy values ranging between 75 and 91%[39,86–89]. Sunil et al.[90] introduced a Multilevel Feature Fusion Network (MFFN) that incorporates ResNet50 and an Adaptive Attention Mechanism to detect diseases in tomato leaves. Their approach achieved a high testing accuracy of 99.83% and included an algorithm for testing and prescribing pesticides, which mirrors the step-by-step detection process developed in the current project. While these works demonstrate promising results, they also underscore the importance of integrating ground-level and aerial analysis to provide comprehensive crop assessments[89].

Furthermore, the application of XAI has been explored in plant disease detection, particularly for banana leaves. In a study conducted by Ashoka et al.[91] XAI was employed to differentiate between healthy leaves and those infected with Black Sigatoka. Similarly, Padilla et al. evaluated the performance of YOLOv8 and YOLOv9 in detecting Fusarium Wilt in banana plants, demonstrating that YOLOv9 outperformed YOLOv8, with mean Average Precision (mAP) scores of 0.66 and 0.61, respectively. These findings align with the current study, where YOLOv9 achieved superior performance over YOLOv8, reinforcing the architecture's robustness for disease detection tasks.

When comparing the overall system to other solutions, several research and commercial projects have attempted to create similar frameworks[42–46]. However, these projects often are not specifically tailored to bananas, lack integration between UAV and ground-level platforms, are limited to specific regions, involve paywalls and limited open access, and frequently do not provide a visual endpoint or an optimized user experience.

Finally, the present work distinguishes itself by integrating recent advancements in deep learning architectures, specifically YOLOv8 and YOLOv9, applied to large-scale datasets collected from both aerial and ground-level sources. Moreover, the incorporation of Explainable AI (XAI) and Human-in-the-Loop AI (HILAI) ensures not only high detection accuracy but also model transparency and iterative refinement, addressing practical challenges in real-world agricultural disease management. This combination of state-of-the-art methodologies highlights the novelty and practical applicability of the current work, setting it apart from existing studies.

Conclusion and future directions

Our proposed surveillance system stands out as a successful example of an end-to-end deep learning pipeline, encompassing all stages from image collection to model deployment. This user-centric system leverages Explainable AI (XAI) and Human-in-the-Loop AI (HILAI) to ensure user-friendliness, precision, and open-access. Through its aerial and ground-level platforms and linked online mapping platform, the system caters to both large-scale and small-scale banana production.

This scalable and real-time monitoring system ensures timely data collection and effective resource allocation, ultimately leading to better management of banana plant diseases. By integrating UAV and ground-level platforms, this framework offers comprehensive surveillance capabilities adaptable to various scales of banana production. The multiplatform approach not only enhances the precision of disease detection but also facilitates swift responses to emerging threats. The Tumaini App, designed with Human-in-the-Loop AI (HILAI) principles, offers a transparent and user-friendly application for disease monitoring. This app, integrated with an online platform for disease mapping, demonstrates a complete solution for disease management, encompassing different opportunities from data collection to real-world applications.

While this work achieved significant advancements, future steps include the development of appropriate implementation policies tailored to each country's National Plant Protection Organization (NPPO). Additionally, there are opportunities to further enhance the models by exploring newer architectures, creating more robust datasets, and employing advanced image processing techniques to improve feature extraction. Transforming these models into

Model	Asia																				
	Rachis			Cut fruit			Whole plant			Leaf			Bunch			Pseudostem			Corm		
Classes	Precision	Recall	F1 Score	Precision	Recall	F1 Score	Precision	Recall	F1 Score	Precision	Recall	F1 Score	Precision	Recall	F1 Score	Precision	Recall	F1 Score	Precision	Recall	F1 Score
Train	0.99	0.98	0.98	0.94	0.91	0.92	0.89	0.79	0.84	0.81	0.79	0.80	0.94	0.95	0.94	0.98	0.98	0.98	0.99	0.99	0.99
Test	0.98	0.98	0.98	0.89	0.86	0.87	0.92	0.76	0.83	0.87	0.65	0.74	0.97	0.92	0.94	0.98	0.98	0.98	0.97	0.98	0.97

Table 16. Precision, recall and F1-Score for ground level models in Asia.

edge computing applications for on-device processing holds significant potential. While real-time detection using UAVs shows promise, further fine-tuning and field testing are required to optimize performance.

Overall, this research lays a strategic foundation for future advancements in crop disease detection and management, with the potential to significantly enhance agricultural practices and contribute to global food security. Looking ahead, we envision AI as a crucial tool for agricultural resilience and early-warning disease management systems, paving the stage for future innovations in crop disease management.

Model	Australia																				
	Rachis			Cut fuit			Whole plant			Leaf			Bunch			Pseudostem			Corm		
Classes	Precision	Recall	F1 Score	Precision	Recall	F1 Score	Precision	Recall	F1 Score	Precision	Recall	F1 Score	Precision	Recall	F1 Score	Precision	Recall	F1 Score	Precision	Recall	F1 Score
Train	0.99	0.98	0.98	0.96	0.92	0.94	0.88	0.78	0.83	0.78	0.71	0.74	0.94	0.91	0.92	0.99	0.97	0.98	0.99	0.99	0.99
Test	0.98	0.98	0.98	0.95	0.91	0.93	0.88	0.82	0.85	0.9	0.65	0.75	0.97	0.88	0.92	0.98	0.97	0.97	0.97	0.98	0.97

Table 17. Precision, recall and F1-Score for ground level models in Australia.

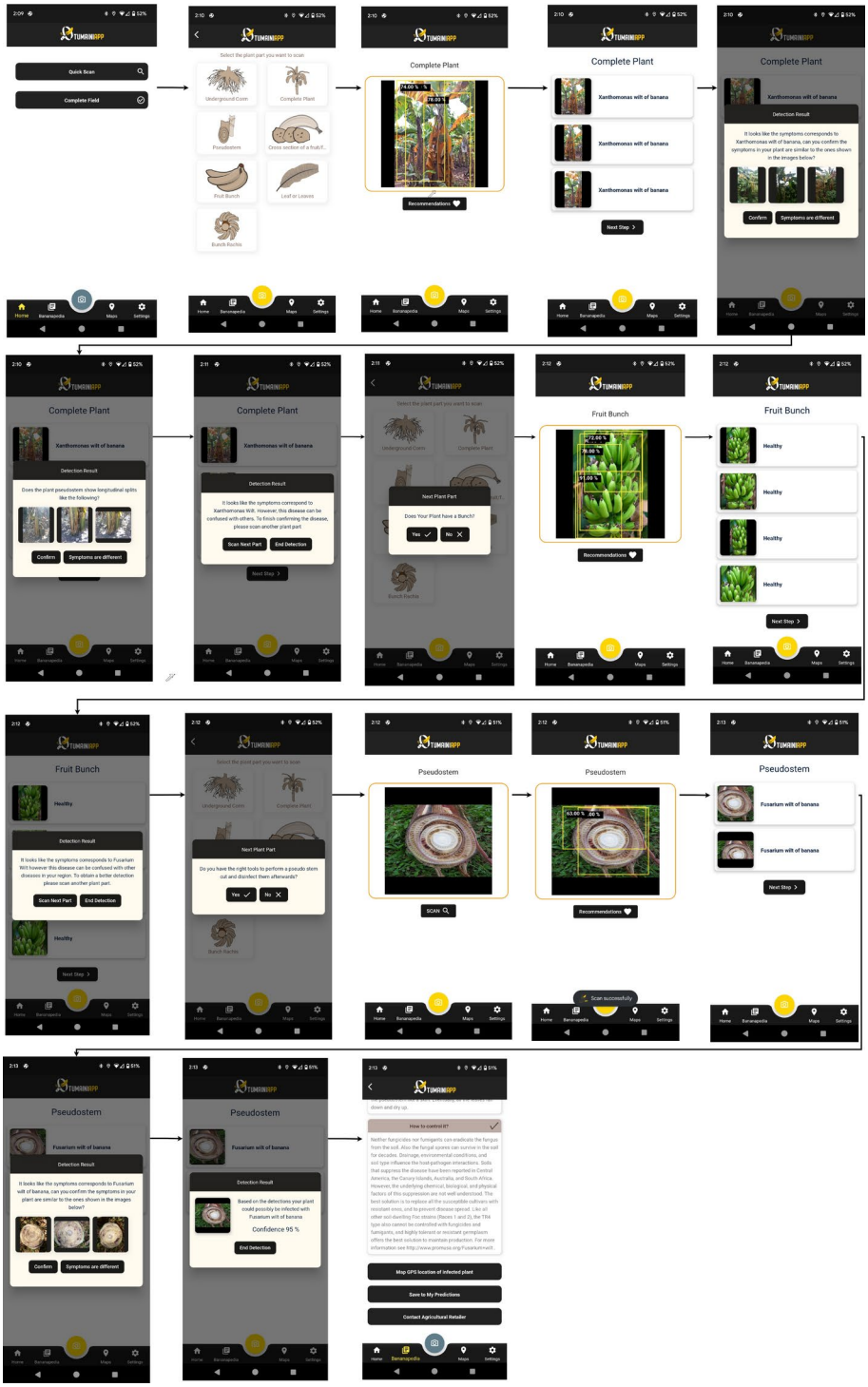

Fig. 7. Step by step process In App.

Disease	Number of plants mapped	Time frame
Healthy	58,446	2007-Present Day
Fusarium Wilt	3772	2021-Present Day
BBTD	2757	2011-Present Day
Xanthomonas Wilt	3583	2007-Present Day
Black Sigatoka	351	2022-Present Day
Moko	25	2022-Present Day
Black Sigatoka + Yellow Sigatoka	1999	2022-Present Day
Total	70,953	

Table 18. Banana database description per class.

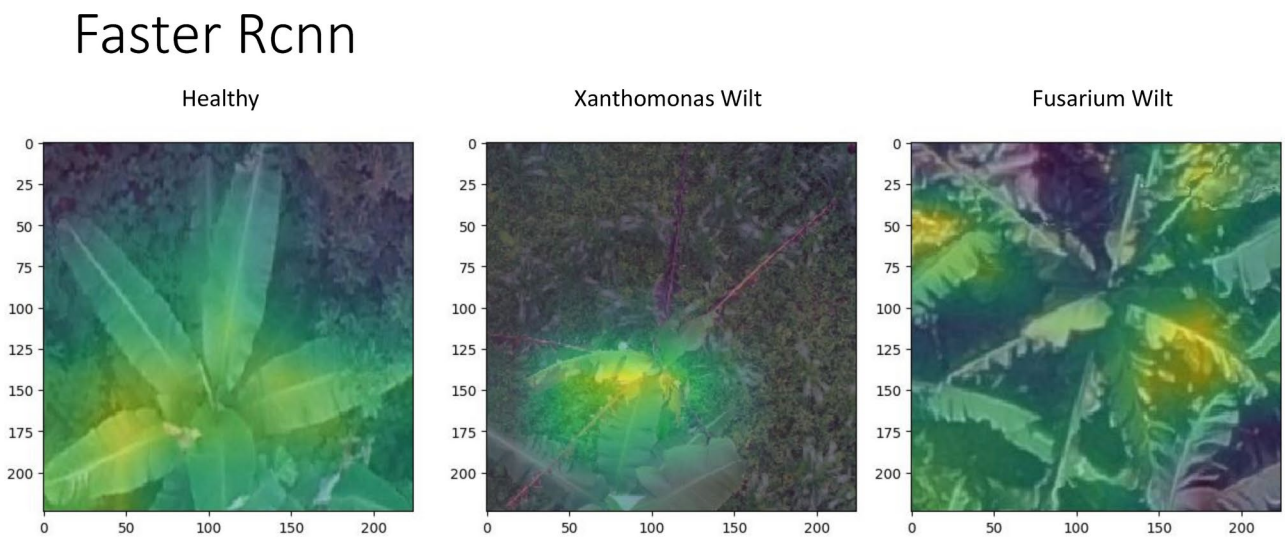

Fig. 8. Gradcam Heatmap for FasterRcnn.

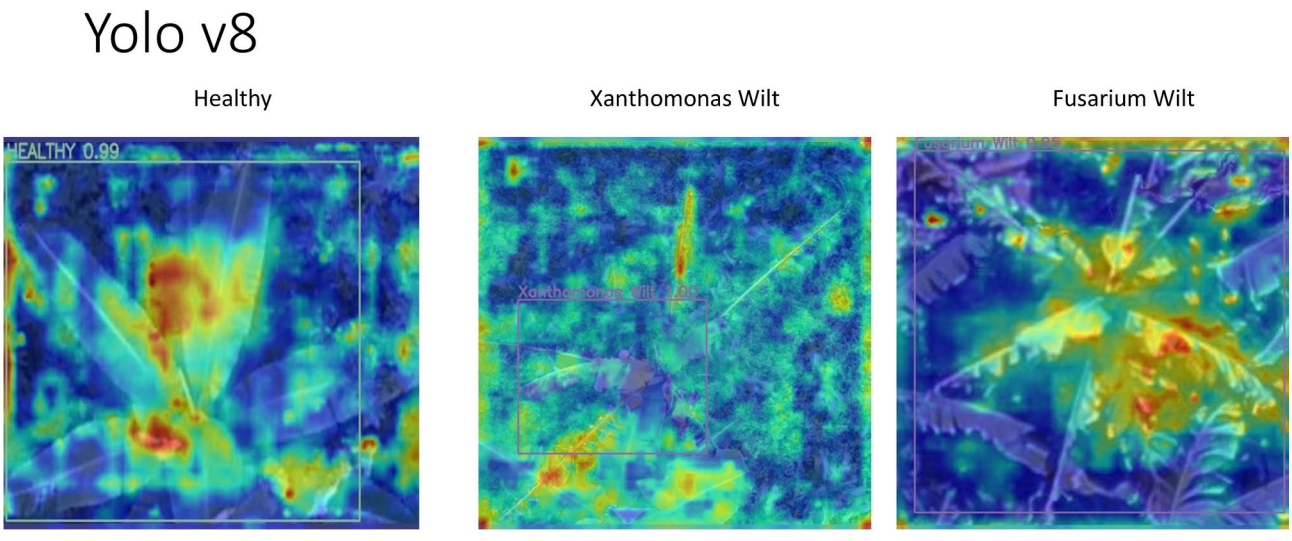

Fig. 9. Gradcam Heatmap for YOLOv8.

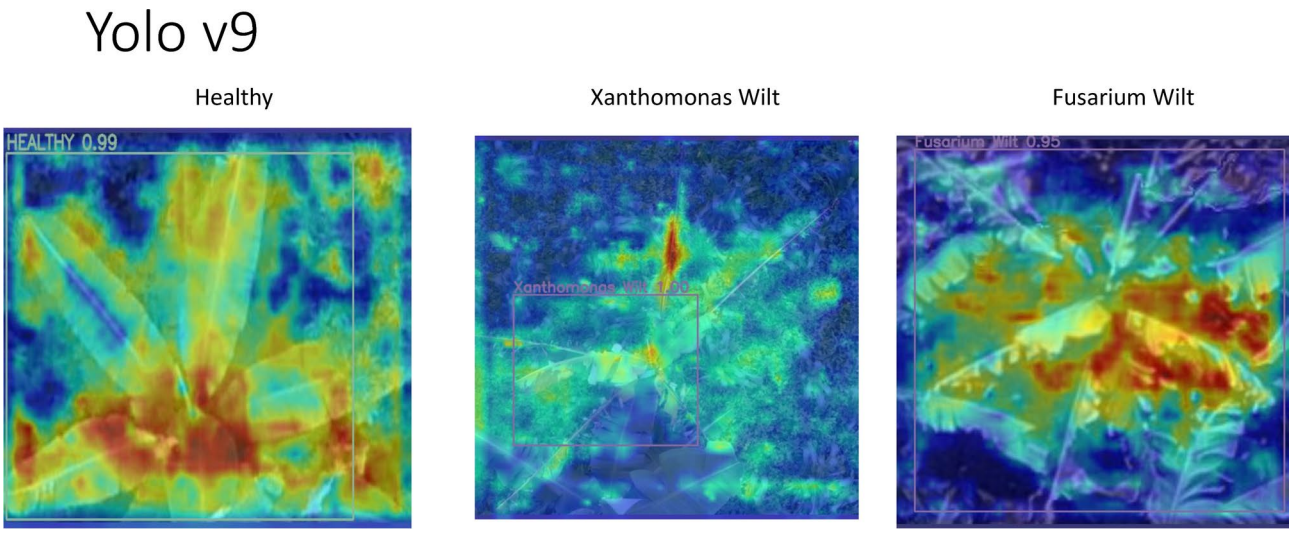

Fig. 10. Gradcam Heatmap for YOLOv9.

Data availability

The datasets used and analyzed during the current study are available from the corresponding author upon request.

Received: 3 September 2024; Accepted: 20 January 2025
Published online: 28 January 2025

References

1. FAOSTAT, Banana and Plantain Surface and Production in 2013. http://faostat.fao.org/site/339/default.aspx.
2. Inafrica24, Bananas from Africa. http://inafrica24.com/modernity/bananas-from-africa/.
3. Martínez-de la Parte, E. et al. Genetic diversity of the banana Fusarium wilt pathogen in Cuba and across Latin America and the Caribbean. *Environ. Microbiol.* https://doi.org/10.1111/1462-2920.16636 (2024).
4. Petsakos, A. et al. Understanding the consequences of changes in the production frontiers for roots, tubers and bananas. *Glob Food Sec* **20**, 180–188. https://doi.org/10.1016/j.gfs.2018.12.005 (2019).
5. FAOSTAT, Crop Production Database. http://www.fao.org/faostat/en/#data/QC. Accessed April 19, 2020; http://www.fao.org/faostat/en/#data/QC
6. Dita, M. A., Garming, H., Van den Bergh, I., Staver, C. & Lescot, T. Banana in Latin America and the Caribbean: Current state, challenges and perspectives. *Acta Hortic.* **986**, 365–380. https://doi.org/10.17660/ActaHortic.2013.986.39 (2013).
7. Government of Western Australia Department of Primary Industries and Regional Development's. Agriculture and Food, Bananas, https://www.agric.wa.gov.au/crops/horticulture/fruit/bananas
8. Singh, H.P., Uma, S., Selvarajan, R. and Karihaloo, J.L., Micropropagation for production of quality banana planting material in Asia-Pacific. In *Asia-Pacific Consortium on Agricultural Biotechnology (APCoAB), New Delhi, India*, vol. 92, (2011).
9. Fuller, D. Q. & Madella, M. *Banana Cultivation in South Asia and East Asia: A Review of the Evidence from Archaeology and Linguistics*. (2009).
10. Alabi, T. R., Adewopo, J., Duke, O. P. & Kumar, P. L. Banana mapping in heterogenous smallholder farming systems using high-resolution remote sensing imagery and machine learning models with implications for banana bunchy top disease surveillance. *Remote Sens.* **14**(20), 5206. https://doi.org/10.3390/rs14205206 (2022).
11. Lokossou, B. et al. Occurrence of Banana bunchy top virus in banana and plantain (Musa sp.) in Benin. *New Dis. Rep.* **25**(1), 13–13. https://doi.org/10.5197/j.2044-0588.2012.025.013 (2012).
12. Quinn, J., Leyton-Brown, K. & Mwebaze, E. *Modeling and Monitoring Crop Disease in Developing Countries.*, vol. 2. (2011).
13. Barbedo, J. A review on the use of unmanned aerial vehicles and imaging sensors for monitoring and assessing plant stresses. *Drones* **3**(2), 40. https://doi.org/10.3390/drones3020040 (2019).
14. Gomez Selvaraj, M. et al. Detection of banana plants and their major diseases through aerial images and machine learning methods: A case study in DR Congo and Republic of Benin. *ISPRS J. Photogramm. Remote Sens.* **169**, 110–124. https://doi.org/10.1016/j.isprsjprs.2020.08.025 (2020).
15. Alvarez-Mendoza, C. I. et al. Predictive modeling of above-ground biomass in brachiaria pastures from satellite and UAV imagery using machine learning approaches. *Remote Sens.* **14**(22), 5870. https://doi.org/10.3390/rs14225870 (2022).
16. Shahi, T. B., Xu, C.-Y., Neupane, A. & Guo, W. Recent advances in crop disease detection using UAV and deep learning techniques. *Remote Sens.* **15**(9), 2450. https://doi.org/10.3390/rs15092450 (2023).
17. Jiang, F., Lu, Y., Chen, Y., Cai, D. & Li, G. Image recognition of four rice leaf diseases based on deep learning and support vector machine. *Comput. Electron Agric.* **179**, 105824. https://doi.org/10.1016/j.compag.2020.105824 (2020).
18. Zhang, D. et al. Detection of rice sheath blight using an unmanned aerial system with high-resolution color and multispectral imaging. *PLoS One* **13**(5), e0187470. https://doi.org/10.1371/journal.pone.0187470 (2018).
19. Bari, B. S. et al. A real-time approach of diagnosing rice leaf disease using deep learning-based faster R-CNN framework. *PeerJ Comput. Sci.* **7**, e432. https://doi.org/10.7717/peerj-cs.432 (2021).
20. Johannes, A. et al. Automatic plant disease diagnosis using mobile capture devices, applied on a wheat use case. *Comput. Electron Agric.* **138**, 200–209. https://doi.org/10.1016/j.compag.2017.04.013 (2017).
21. Velumani, K. et al. Estimates of maize plant density from UAV RGB images using faster-RCNN detection model: Impact of the spatial resolution. *Plant Phenom.* https://doi.org/10.34133/2021/9824843 (2021).

22. Khalid, A., Akbar, S., Hassan, S. A., Firdous, S. & Gull, S., Detection of tomato leaf disease using deep convolutional neural networks. In *2023 4th International Conference on Advancements in Computational Sciences (ICACS)*, 1–6 (IEEE, 2023), https://doi.org/10.1109/ICACS55311.2023.10089689.
23. Nawaz, M. et al. A robust deep learning approach for tomato plant leaf disease localization and classification. *Sci. Rep.* **12**(1), 18568. https://doi.org/10.1038/s41598-022-21498-5 (2022).
24. Çetiner, H. Citrus disease detection and classification using based on convolution deep neural network. *Microprocess Microsyst.* **95**, 104687. https://doi.org/10.1016/j.micpro.2022.104687 (2022).
25. Selvaraj, M. G. et al. Machine learning for high-throughput field phenotyping and image processing provides insight into the association of above and below-ground traits in cassava (*Manihot esculenta* Crantz). *Plant Methods* https://doi.org/10.21203/rs.2.24148/v3 (2020).
26. Amarasingam, N., Gonzalez, F., Salgadoe, A. S. A., Sandino, J. & Powell, K. Detection of white leaf disease in sugarcane crops using UAV-derived RGB imagery with existing deep learning models. *Remote Sens.* **14**(23), 6137. https://doi.org/10.3390/rs14236137 (2022).
27. Lu, Y., Yi, S., Zeng, N., Liu, Y. & Zhang, Y. Identification of rice diseases using deep convolutional neural networks. *Neurocomputing* **267**, 378–384. https://doi.org/10.1016/J.NEUCOM.2017.06.023 (2017).
28. Sudhesh, K. M., Sowmya, V., Sainamole Kurian, P. & Sikha, O. K. AI based rice leaf disease identification enhanced by dynamic mode decomposition. *Eng. Appl. Artif. Intell.* **120**, 105836. https://doi.org/10.1016/J.ENGAPPAI.2023.105836 (2023).
29. Selvaraj, M. G. et al. AI-powered banana diseases and pest detection. *Plant Methods* **15**(1), 92. https://doi.org/10.1186/s13007-019-0475-z (2019).
30. Ani Brown Mary, N., Robert Singh, A. & Athisayamani, S. Classification of banana leaf diseases using enhanced gabor feature descriptor, 229–242 (2021). https://doi.org/10.1007/978-981-15-7345-3_19.
31. Chaudhari, V. & Patil, M. Banana leaf disease detection using K-means clustering and Feature extraction techniques. In *2020 International Conference on Advances in Computing, Communication & Materials (ICACCM)* 126–130 (IEEE, 2020). https://doi.org/10.1109/ICACCM50413.2020.9212816.
32. Genet, Y. H., Sinshaw, N. T., Assefa, B. G. & Mohapatra, S. K. Sigatoka and xanthomonas banana leaf disease detection via transfer learning. *Sci. Iran.* **0**(0), 0–0. https://doi.org/10.24200/sci.2024.62306.7766 (2024).
33. Sangeetha, R., Logeshwaran, J., Rocher, J. & Lloret, J. An improved agro deep learning model for detection of panama wilts disease in banana leaves. *AgriEngineering* **5**(2), 660–679. https://doi.org/10.3390/agriengineering5020042 (2023).
34. R. Bommasani et al. On the opportunities and risks of foundation models. (2021).
35. Vo, H.-T., Mui, K. C., Thien, N. N. & Tien, P. P. Automating tomato ripeness classification and counting with YOLOv9. *Int. J. Adv. Comput. Sci. Appl.* https://doi.org/10.14569/IJACSA.2024.01504113 (2024).
36. Calou, V. B. C. et al. The use of UAVs in monitoring yellow sigatoka in banana. *Biosyst. Eng.* **193**, 115–125. https://doi.org/10.1016/j.biosystemseng.2020.02.016 (2020).
37. Ani Brown Mary, N., Robert, S. A. & Athisayamani, S. Banana leaf diseased image classification using novel HEAP auto encoder (HAE) deep learning. *Multimed. Tools Appl.* **79**(41–42), 30601–30613. https://doi.org/10.1007/s11042-020-09521-1 (2020).
38. Neupane, B., Horanont, T. & Hung, N. D. Deep learning based banana plant detection and counting using high-resolution red-green-blue (RGB) images collected from unmanned aerial vehicle (UAV). *PLoS One* **14**(10), e0223906. https://doi.org/10.1371/journal.pone.0223906 (2019).
39. Mora, J. J., Selvaraj, M. G., Alvarez, C. I., Safari, N. & Blomme, G. From pixels to plant health: Accurate detection of banana *Xanthomonas* wilt in complex African landscapes using high-resolution UAV images and deep learning. *Discov. Appl. Sci.* **6**(7), 377. https://doi.org/10.1007/s42452-024-06073-z (2024).
40. Zhang, S. et al. Banana fusarium wilt disease detection by supervised and unsupervised methods from UAV-based multispectral imagery. *Remote Sens.* **14**(5), 1231. https://doi.org/10.3390/rs14051231 (2022).
41. Aliff, M. et al. Utilizing aerial imagery and deep learning techniques for identifying banana plants diseases. *ITM Web Conf.* **60**, 00013. https://doi.org/10.1051/itmconf/20246000013 (2024).
42. Cuéllar, W. J. et al. PestDisPlace; Monitoring the distribution of pests and diseases. Version 1.0. (2018).
43. Agrocalidad, Estamos Alerta. https://www.estamosalerta.com/#Inicio.
44. Inc. EOS Data Analytics, Solutions. https://eos.com/solutions-tags/agriculture/.
45. PEAT GmbH, Plantix. https://plantix.net/en/.
46. Saillog LTD, Agrio App. https://agrio.app/.
47. Carvajal-Yepes, M. et al. A global surveillance system for crop diseases. *Science* **364**(6447), 1237–1239 (2019).
48. Mora, J. J., Selvaraj, M. G., Alvarez, C. I., Safari, N. & Blomme, G. from pixels to plant health: Accurate detection of banana *Xanthomonas* wilt in complex african landscapes using high-resolution UAV images and deep learning. *Discov. Appl. Sci.* **6**(7), 377 (2024).
49. Mosqueira-Rey, E., Hernández-Pereira, E., Alonso-Ríos, D., Bobes-Bascarán, J. & Fernández-Leal, Á. Human-in-the-loop machine learning: a state of the art. *Artif. Intell. Rev.* **56**(4), 3005–3054. https://doi.org/10.1007/s10462-022-10246-w (2023).
50. Bhatt, N. & Varma, S. Classify-imbalance data sets in IoT framework of agriculture field with multivariate sensors using centroid-based oversampling method. *Natl. Acad. Sci. Lett.* **28**(11), 585–590. https://doi.org/10.1007/s40009-023-01249-4 (2023).
51. Shorten, C. & Khoshgoftaar, T. M. A survey on image data augmentation for deep learning. *J. Big Data* **6**(1), 60. https://doi.org/10.1186/s40537-019-0197-0 (2019).
52. Tanaka, F. H. K. D. S. & Aranha, C. Data augmentation using GANs. *Proc. Mach Learn Res.* **1**, 1–16 (2019).
53. Terven, J. & Córdova-Esparza, D. A comprehensive review of YOLO architectures in computer vision: From YOLOv1 to YOLOv8 and YOLO-NAS. *Mach. Learn. Knowl. Extr.* **5**(4), 1680–1716. https://doi.org/10.3390/make5040083 (2023).
54. Wang, C. -Y., Yeh, I. H., & Mark Liao, H. Y. YOLOv9: Learning What You Want to Learn Using Programmable Gradient Information. (2024).
55. Deci AI research team, YOLO-NAS by Deci Achieves State-of-the-Art Performance on Object Detection Using Neural Architecture Search. https://deci.ai/blog/yolo-nas-object-detection-foundation-model/.
56. Ren, S., He, K., Girshick, R. & Sun, J. Faster R-CNN: Towards real-time object detection with region proposal networks. *IEEE Trans. Pattern Anal. Mach. Intell.* **39**(6), 1137–1149. https://doi.org/10.1109/TPAMI.2016.2577031 (2017).
57. Gunning, D. Explainable artificial intelligence (xAI). Tech. rep., Defense Advanced Research Projects Agency (DARPA). https://www.darpa.mil/program/explainable-artificial-intelligence.
58. Selvaraju, R. R. et al. Grad-CAM: Visual explanations from deep networks via gradient-based localization. *Int. J. Comput. Vis.* **128**(2), 336–359. https://doi.org/10.1007/s11263-019-01228-7 (2020).
59. Das, A. & Rad, P. Opportunities and challenges in explainable artificial intelligence (XAI): A Survey. (2020).
60. Gomez, D. et al. Advancing common bean (*Phaseolus vulgaris* L.) disease detection with YOLO driven deep learning to enhance agricultural AI. *Sci. Rep.* **14**(1), 15596. https://doi.org/10.1038/s41598-024-66281-w (2024).
61. Tao, L., Dong, M. & Xu, C. Dual focal loss for calibration. In *International Conference on Machine Learning*, 33833–33849 (PMLR, 2023)
62. Romero, H. & Morales Acosta, A. A review: Comparison of performance metrics of pretrained models for object detection using the TensorFlow framework. *IOP Conf. Ser. Mater. Sci. Eng.* **844**, 012024. https://doi.org/10.1088/1757-899X/844/1/012024 (2020).
63. Wu, S., Li, X. & Wang, X. IoU-aware single-stage object detector for accurate localization. *Image Vis. Comput* **97**, 103911. https://doi.org/10.1016/j.imavis.2020.103911 (2020).

64. Stewart, E. et al. Quantitative phenotyping of northern leaf blight in UAV images using deep learning. *Remote Sens.* **11**, 2209. https://doi.org/10.3390/rs11192209 (2019).
65. Mao, J., Tian, W., Li, P., Wei, T. & Liang, Z. Phishing-alarm: Robust and efficient phishing detection via page component similarity. *IEEE Access* **5**, 17020–17030. https://doi.org/10.1109/ACCESS.2017.2743528 (2017).
66. Li, Q. et al. A survey on text classification: From traditional to deep learning. *ACM Trans. Intell. Syst. Technol.* **13**(2), 1–41 (2022).
67. Alliance Bioversity Ciat, M. S. TumainiAPP. *Alliance Bioversity Ciat, Palmira, Colombia*. (2019)
68. Blomme, G. et al. Bacterial diseases of bananas and Enset: Current state of knowledge and integrated approaches toward sustainable management. *Front. Plant Sci.* https://doi.org/10.3389/fpls.2017.01290 (2017).
69. Kumar, Y. & Kumar, P. Comparative study of YOLOv8 and YOLO-NAS for agriculture application. In *2024 11th International Conference on Signal Processing and Integrated Networks (SPIN)*, 72–77 (IEEE, 2024). https://doi.org/10.1109/SPIN60856.2024.10511673.
70. Slimani, H., El Mhamdi, J. & Jilbab, A. Advancing disease identification in fava bean crops: A novel deep learning solution integrating YOLO-NAS for precise rust. *J. Intell. Fuzzy Syst.* **46**, 1–15. https://doi.org/10.3233/JIFS-236154 (2023).
71. Mai, X., Zhang, H. & Meng, M. Q.-H. Faster R-CNN with classifier fusion for small fruit detection. In *2018 IEEE International Conference on Robotics and Automation (ICRA)*, 7166–7172 (IEEE, 2018). https://doi.org/10.1109/ICRA.2018.8461130.
72. Cynthia, S. T., Hossain, K. M. S., Hasan, M. N., Asaduzzaman, M., & Das, A. K. Automated detection of plant diseases using image processing and faster r-cnn algorithm. In *2019 International Conference on Sustainable Technologies for Industry 4.0 (STI)*, 1–5 (IEEE, 2019). https://doi.org/10.1109/STI47673.2019.9068092.
73. Ghoury, S., Sungur, C. & Durdu, A. Real-time diseases detection of grape and grape leaves using faster R-CNN and SSD MobileNet architectures. In *International Conference on Advanced Technologies, Computer Engineering and Science (ICATCES 2019), Alanya, Turkey*, 39–44 (2019)
74. Terven, J., Córdova-Esparza, D.-M. & Romero-González, J.-A. A comprehensive review of YOLO architectures in computer vision: From YOLOv1 to YOLOv8 and YOLO-NAS. *Mach Learn Knowl Extr* **5**(4), 1680–1716. https://doi.org/10.3390/make5040083 (2023).
75. Alkentar, S. M., Alsahwa, B., Assalem, A. & Karakolla, D. Practical comparation of the accuracy and speed of YOLO, SSD and Faster RCNN for drone detection. *J. Eng.* **27**(8), 19–31 (2021).
76. Breive, V. & Sledevic, T. Person detection in thermal images: A comparative analysis of YOLOv8 and YOLOv9 models. In *2024 IEEE Open Conference of Electrical, Electronic and Information Sciences (eStream)*, 1–4 (2024). https://doi.org/10.1109/eStream61684.2024.10542600.
77. Bjerge, K., Mann, H. M. R. & Høye, T. T. Real-time insect tracking and monitoring with computer vision and deep learning. *Remote Sens. Ecol. Conserv.* **8**(3), 315–327 (2022).
78. Safaldin, M., Zaghden, N. & Mejdoub, M. An improved YOLOv8 to detect moving objects. *IEEE Access* **12**, 59782–59806. https://doi.org/10.1109/ACCESS.2024.3393835 (2024).
79. Sun, S. et al. Multi-YOLOv8: An infrared moving small object detection model based on YOLOv8 for air vehicle. *Neurocomputing* **588**, 127685. https://doi.org/10.1016/j.neucom.2024.127685 (2024).
80. Zhai, X., Huang, Z., Li, T., Liu, H. & Wang, S. YOLO-drone: An optimized YOLOv8 network for tiny UAV object detection. *Electronics* **12**(17), 3664. https://doi.org/10.3390/electronics12173664 (2023).
81. Gil-Bazan, A. et al. On the Use of YOLO-NAS and YOLOv8 for the detection of sea lions in the Galapagos islands. In *2023 IEEE International Autumn Meeting on Power, Electronics and Computing (ROPEC)*, 1–6 (IEEE, 2023). https://doi.org/10.1109/ROPEC58757.2023.10409394.
82. Casas, E., Ramos, L., Bendek, E. & Rivas-Echeverría, F. Assessing the effectiveness of YOLO architectures for smoke and wildfire detection. *IEEE Access* **11**, 96554–96583. https://doi.org/10.1109/ACCESS.2023.3312217 (2023).
83. Siddiqui, B. S., Mridul, Z. A., Habib, Z., Sakib, I. & Chowdhury, M. A. I. *Real-time foul Detection in Football Matches Using Machine Learning Techniques* (Brac University, 2024).
84. Jati, H., Ilyasa, N. A. & Dominic, D. D. Enhancing humanoid robot soccer ball tracking, goal alignment, and robot avoidance using YOLO-NAS. *J. Robot. Control* **5**(3), 829–838 (2024).
85. Rakesh, S. & Indiramma, M. Explainable AI for crop disease detection. In *2022 4th International Conference on Advances in Computing, Communication Control and Networking (ICAC3N)*, 1601–1608 (IEEE, 2022). https://doi.org/10.1109/ICAC3N56670.2022.10074303.
86. Mathew, M. P. & Mahesh, T. Y. Leaf-based disease detection in bell pepper plant using YOLO v5. *Signal Image Video Process.* **16**(3), 841–847. https://doi.org/10.1007/s11760-021-02024-y (2022).
87. Adem, K., Ozguven, M. M. & Altas, Z. A sugar beet leaf disease classification method based on image processing and deep learning. *Multimed. Tools Appl.* **82**(8), 12577–12594. https://doi.org/10.1007/s11042-022-13925-6 (2023).
88. Padilla, J. I. A., Pastor, H. M. R., Velasco, A. C. T. & Magsumbol, J. A. V. Performance evaluation of YOLOv8, YOLOv9 and YOLOv10 models in detecting fusarium wilt disease in banana leaf plants. In *2024 IEEE International Conference on Imaging Systems and Techniques (IST)*, 1–7 (IEEE, 2024)
89. Sunil, C. K., Jaidhar, C. D. & Patil, N. Systematic study on deep learning-based plant disease detection or classification. *Artif. Intell. Rev.* **56**(12), 14955–15052. https://doi.org/10.1007/s10462-023-10517-0 (2023).
90. Sunil, C. K., Jaidhar, C. D. & Patil, N. Tomato plant disease classification using Multilevel Feature Fusion with adaptive channel spatial and pixel attention mechanism. *Expert. Syst. Appl.* **228**, 120381. https://doi.org/10.1016/j.eswa.2023.120381 (2023).
91. A. B et al., *Explainable AI Based framework for Banana Disease Detection*. (2024). https://doi.org/10.21203/rs.3.rs-4125300/v1.

Acknowledgements

The authors would also like to acknowledge Jorge Eliecer Vargas and Dr Miguel Dita for helping us establish partners to enhance data collection as well as reviewing our app and helping us improve it. We are highly thankful for the work done by Juan Carlos Rojas, Hugo Banegas, Giovana Fonseca, and Dr Ahn Nguyen for helping us collect data in Perú, Ecuador, and Vietnam respectively. Thanks to Angela Fernando, CIAT consultant, for formatting and technical editing of the manuscript. Bioversity International provided funding for field UAV image collection in the framework of the Roots, Tubers and Bananas program. We thank the RTB Program Management Unit, the German Corporation for International Cooperation (GIZ) and the Plant Health Initiative that supported this study and the CGIAR Fund Donors (https://www.cgiar.org/funders/).

Author contributions

J.M., M.G.S., and G. B. designed the study and performed the experiments and are the main contributing authors of the paper. N. S., contributed to the image collection of UAV images and expert pre-screening of symptoms in hotspots. S.E. and R.S. contributed to identification and confirmation of diseases as well testing and validation of the Tumaini App in India.

Declarations

Competing interests
The authors declare no competing interests.

Consent for publication
All authors agreed to publish this manuscript.

Research involving plant statement
The authors affirm that all requisite permissions and licenses for the collection of plant and all plant parts and their accompanying images, utilized in this study, have been duly obtained in adherence to relevant regulations and guidelines. Additionally, the authors confirm that the species utilized in this study are not endangered.

Additional information
Supplementary Information The online version contains supplementary material available at https://doi.org/10.1038/s41598-025-87588-2.

Correspondence and requests for materials should be addressed to M.G.S.

Reprints and permissions information is available at www.nature.com/reprints.

Publisher's note Springer Nature remains neutral with regard to jurisdictional claims in published maps and institutional affiliations.